Bioactive Materials 50 (2025) 215–231

Contents lists available at ScienceDirect

Bioactive Materials

journal homepage: www.keaipublishing.com/en/journals/bioactive-materials

All-in-one extracellular matrix-based powders with instant self-assembly and multiple bioactivities integrate hemostasis and in-situ tissue functional repair

Chen-Yu Zou [a,b,1], Chen Han [a,b,1], Ming Xiong [a,c], Juan-Juan Hu [a,c], Yan-Lin Jiang [a,b], Xiu-Zhen Zhang [a,b], Ya-Xing Li [a,b], Long-Mei Zhao [a,b], Yu-Ting Song [a,b], Qing-Yi Zhang [a,b], Qian-Jin Li [a,b], Rong Nie [a,b], Yue-Qi Zhang [a,b], Jesse Li-Ling [a,b,d], Hui-Qi Xie [a,b,*]

[a] Department of Orthopedic Surgery and Orthopedic Research Institute, Stem Cell and Tissue Engineering Research Center, State Key Laboratory of Biotherapy, West China Hospital, Sichuan University, Chengdu, Sichuan, 610041, PR China
[b] Tianfu Jincheng Laboratory, Chengdu, Sichuan, 610093, PR China
[c] Department of Otolaryngology, Head and Neck Surgery, West China Hospital, Sichuan University, Chengdu, Sichuan, 610041, PR China
[d] Department of Medical Genetics, West China Second Hospital, Sichuan University, Chengdu, Sichuan, 610041, PR China

ARTICLE INFO

Keywords:
Extracellular matrix
Wet adhesion
Self-assembly
Non-compressible hemorrhage
Tissue repair

ABSTRACT

Non-compressible hemorrhage poses a severe threat to life globally, yet achieving effective hemostasis and facilitating tissue repair remain a significant challenge and desired requirement. Herein, the all-in-one extracellular matrix (ECM)-based powder, composed of modified small intestinal submucosa (SIS) and sodium alginate, was ingeniously designed to realize one-stop management for non-compressible hemorrhage. Specifically, upon contact bleeding site, the powder's extreme liquid absorption allows for the rapid removal of interfacial blood. Simultaneously, based on the instant self-assembly strategy of covalent/non-covalent interaction, the powder can transform to wet bio-adhesive hydrogel within 5 s, effectively sealing the wound. Using the inherent bioactivities, the ECM-based powder exhibits satisfactory biocompatibility, enhanced cell recruitment, angiogenesis and endothelial cell functions. Ulteriorly, excellent hemostasis performance have verified in rabbit liver non-compressible hemorrhage and heart/artery massive hemorrhage models, significantly reducing the blood loss. More importantly, after hemostasis, the impaired liver demonstrates functional restoration that the more vessels and bile ducts formation, facilitated by the biodegradation of ECM-derived powders *in vivo* and the multi-biological cues response. Collectively, leveraging the merits of powder and hydrogel, this novel powder fulfills the all-in-one need for both non-compressible hemorrhage control and subsequent tissue repair, signifying it a valuable material in first aid.

1. Introduction

Uncontrolled hemorrhage has emerged as a significant cause of mortality, accounting for 30 % of trauma-related deaths in military combat or civilian setting, making it a critical concern. Notably, approximately 50 % of such fatalities are potentially preventable with immediate emergency intervention [1,2]. To this end, various hemostatic measures have been developed such as tourniquets, clotting factors and antifibrinolytic agent, but challenges persist in managing massive non-compressible hemorrhage occurring in the body trunk and internal organs [3,4]. Thereby, the development of materials for non-compressible hemorrhage remains an exceedingly challenge.

Powder-type materials, characterized by their large specific surface area and superior liquid absorption capacity, are particularly advantageous for deep and irregular bleeding sites compared to other materials such as gauzes, hydrogels, and sponges. Nevertheless, lacking bio-

Peer review under the responsibility of editorial board of Bioactive Materials.
* Corresponding author. Department of Orthopedic Surgery and Orthopedic Research Institute, Stem Cell and Tissue Engineering Research Center, State Key Laboratory of Biotherapy, West China Hospital, Sichuan University, Chengdu, Sichuan, 610041, PR China.
E-mail addresses: jliling@scu.edu.cn (J. Li-Ling), xiehuiqi@scu.edu.cn (H.-Q. Xie).
[1] These authors contributed equally to this work.

https://doi.org/10.1016/j.bioactmat.2025.04.005
Received 26 December 2024; Received in revised form 3 April 2025; Accepted 3 April 2025

adhesion and dispersion in blood have been obstacles for traditional hemostatic powders (e.g., QuickClot®, Celox™) to use in non-compressible hemorrhage control [5–7]. Self-assembly, generally refers to the spontaneous formation of an ordered structure from a basic unit, has gained increasing attention in hemostasis and tissue repair [8–11]. As reported, the hemostatic powders with self-assembly can achieve powder-hydrogel transformation [12,13]. For example, Bian's group developed a PEI/PAA/QCS powder that could form a stable physical barrier to seal wounds within 4 s upon hydration [14]. Moreover, a gelable and adhesive powder (GAP) based on chitosan and modified poly(ethylene glycol) is developed by Wu's group. It could turns into wet-adhesive hydrogel via covalent bonding [15]. There innovative designs combined the advantages of both powders and hydrogels. Additionally, hydrogels, with their biomimetic 3D structure, have shown promise in promoting tissue repair across various fields, although this aspect has not been fully explored in self-assembling powders [16–18]. Moreover, ideal hemostatic materials should not only meet the hemostatic effect, but also consider biodegradability *in vivo* and support tissue repair after hemostasis [19,20].

Extracellular matrix (ECM) materials, derived from human or animal tissues after removing immunogenic components, have gained significant attention [21,22]. Small intestinal submucosa (SIS), an FDA-approved ECM material, has found widespread application in multiple areas [23,24]. In our preliminary studies, a series of biodegradable and bioactive SIS-based materials have been applied to foster multiple tissue repair such as skin, urethra, bone and vocal folds [25–30]. Thoroughly, profited from inherent biological and mechanical cues, many biological processes such as immunomodulation, endogenous stem cell recruitment, and epithelial regeneration have been demonstrated in SIS-tissue interaction [31,32]. Moreover, the rich functional groups present in SIS also provide convenience for functional modification [33]. Given these advantages, SIS holds great potential in the development of novel hemostatic and tissue repair materials.

Inspired by these, we have designed an ECM-based powders composed of modified SIS and sodium alginate for tissue functional repair after controlling non-compressible bleeding (Scheme 1). Upon touching the bleeding site, based on its excellent hydrophilicity and self-healing capacity, the powders can absorb interfacial blood and simultaneously complete the self-assembly within 5 s. Subsequently, the formed ECM-based hydrogels exhibit robust wet bio-adhesion, effectively sealing the wound. Additionally, profited from the inherent bioactivity, the material exhibits endothelial cell recruitment and function enhancement. Furthermore, ECM-based powders have excellent hemostasis effects in rabbit non-compressible and massive

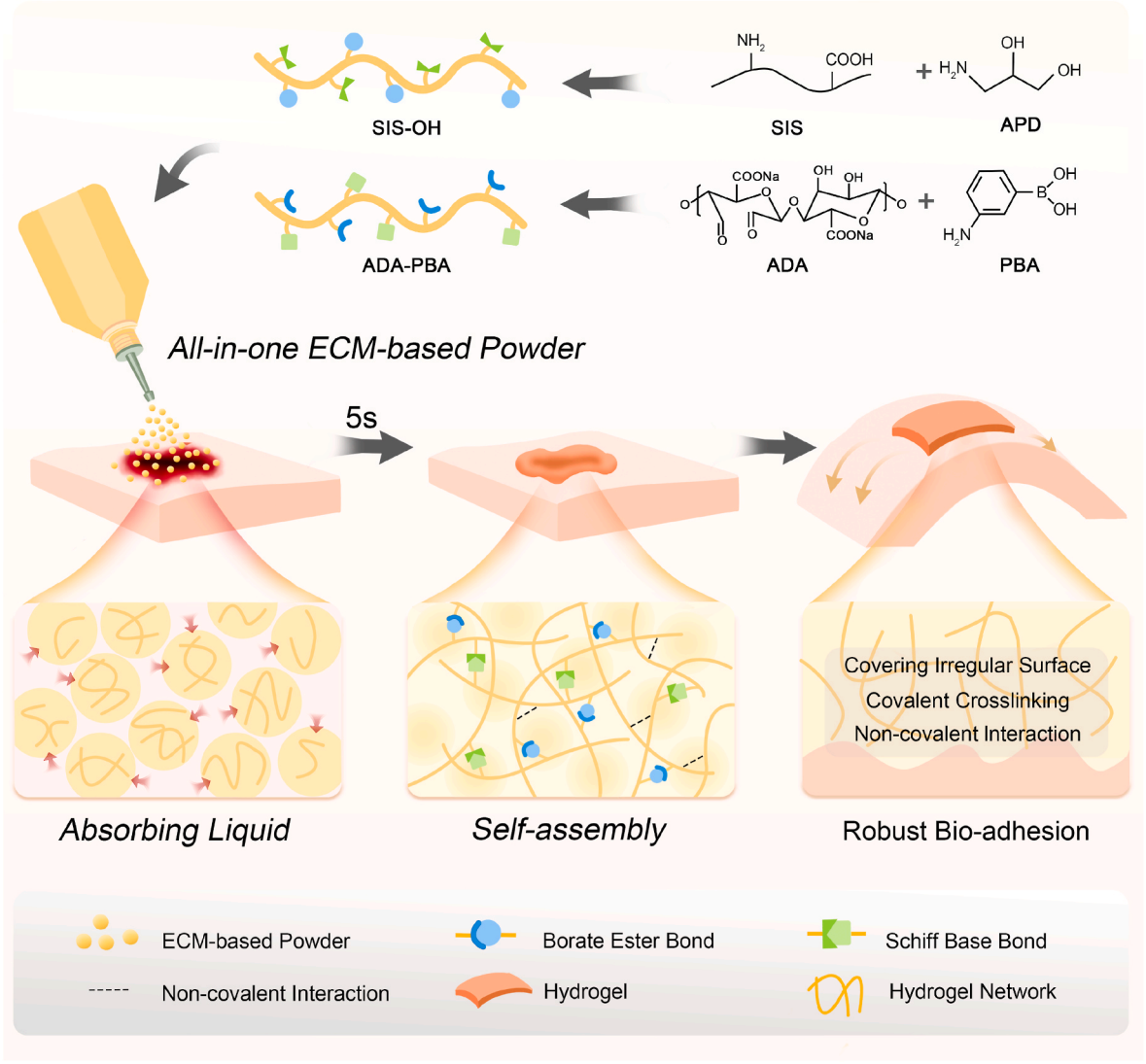

Scheme 1. The design and application of the all-in-one ECM-based powders. This powder is composed of modified SIS and sodium alginate, which can instantly achieve self-assembly within 5 s upon contact the liquid, and finally achieve robust wet bio-adhesion.

hemorrhage models. More importantly, we have demonstrated that, with the material biodegradation *in vivo* after hemostasis, the neovascularization and bile duct formation are promoted, ultimately leading to liver functional repair. Therefore, ECM-based powders are appealing for controlling non-compressible bleeding and tissue functional repair after hemostasis.

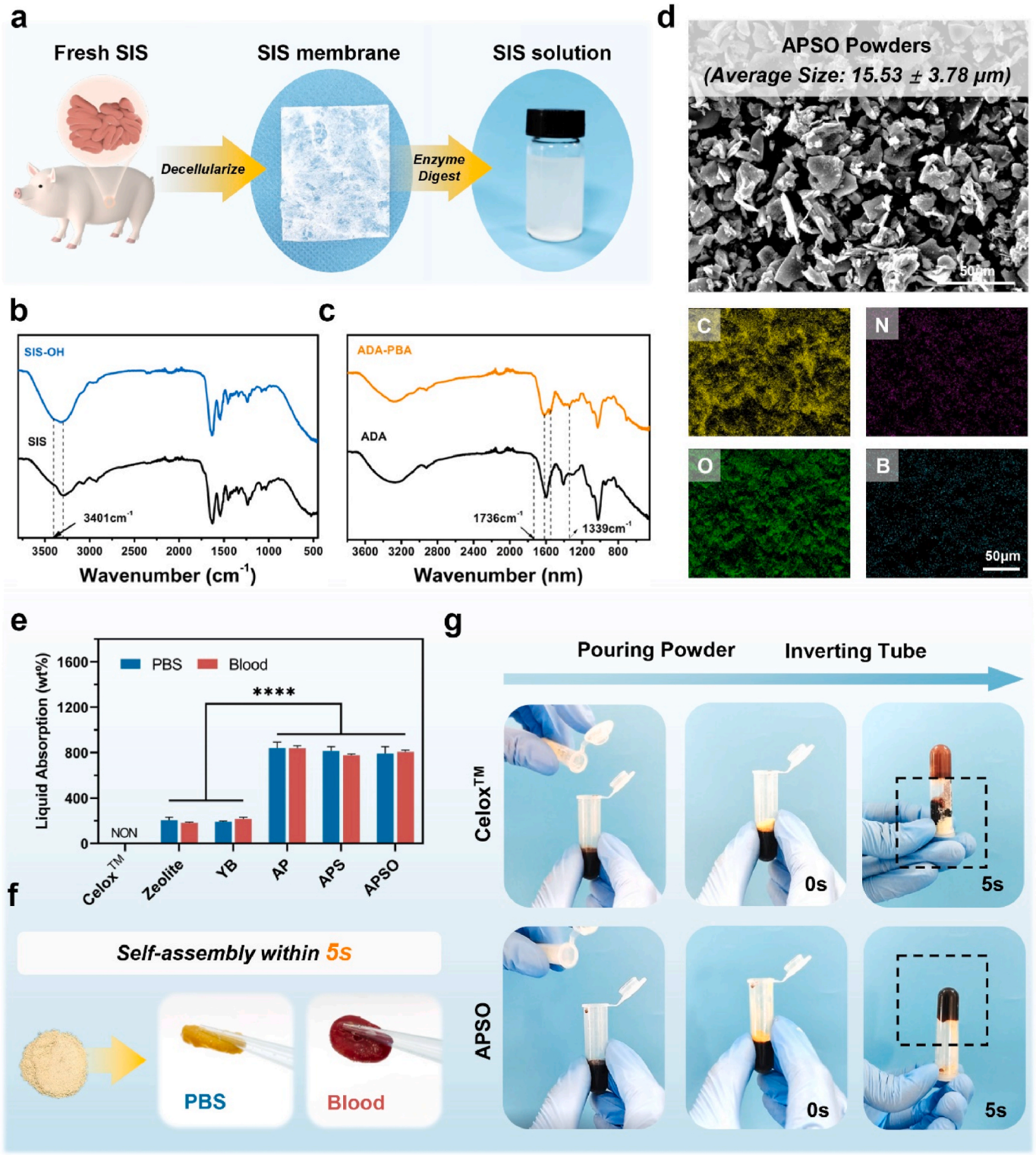

Fig. 1. a) The preparation process of SIS solution, including decellularization and enzyme digest; The FTIR spectra of b) SIS components (SIS, SIS-OH) and c) sodium alginate components (ADA, ADA-PBA); d) The SEM images and elements distribution (C, N, O, B) of APSO powders; e) Liquid absorption (wt%) of AP, APS, APSO and representative commercial hemostatic powders after 5 s; f) The digital images of APSO powders before and after self-assembly; g) The self-assembly effect of APSO and Celox™ powders in anticoagulant blood using inverted tube method (****$P < 0.0001$).

2. Results and discussion

2.1. Preparation and instant self-assembly of ECM-based powders

The decellularized porcine small intestine submucosa, namely SIS, was prepared via multi-step decellularization technique using fresh porcine small intestine. For further functional modification, enzymatic digestion was applied to obtain SIS solution after hydrolyzing the proteins and other components of SIS, but retain their molecular structure (Fig. 1a) [23]. The SIS was hydroxylated by convenient amidation reaction, and an arresting -OH peak at 3401 cm^{-1} was observed on the fourier transform infrared spectroscopy (FTIR) spectrum of SIS-OH (Fig. 1b). The peak (1736 cm^{-1}) attributed to the -CHO group proved the successful synthesis of aldehydeated sodium alginate (ADA). As to ADA-PBA, the obvious absorption peak at 1340 cm^{-1} was ascribed the stretching vibration of B-O bonds in boronophenyl groups (Fig. 1c). These results certificated the successful synthesis of SIS-OH and ADA-PBA, which laid the molecular basis for hydrogel formation.

The ratio of ADA-PBA and SIS-OH was initially determined by rheological properties. As shown in Fig. S1 in Supporting Information, among the four hydrogels with different component volume ratios, the G' of the 2: 1 group (3852 Pa) was the highest, indicating that the hydrogel had a highly cross-linked network. Therefore, a V (ADA-PBA): V (SIS-OH) ratio of 2: 1 was selected for subsequent hemostatic powder preparation. Here, three kinds of ECM-based materials, namely AP, APS and APSO powders, were prepared: 1) AP powders only contain ADA-PBA; 2) APS powders contain ADA-PBA and SIS; 3) APSO powders contain ADA-PBA and SIS-OH. All of them were obtained by convenient physical grinding shown in Fig. S2 in Supporting Information, which facilitates large-scale production. Scanning electron microscopy (SEM) images showed that the morphology of AP, APS and APSO powders was irregular shape with the particle size of 14.55 ± 4.08 μm, 16.09 ± 2.86 μm and 15.72 ± 2.35 μm, respectively (Fig. 1d and S3, Supporting Information). Furthermore, the energy dispersive spectrometer (EDS) images revealed the even distribution of primary elements C, O, N, and B in APSO powders, thereby confirming the uniformity of molecular structure. Shown in Fig. S4 in Supporting Information, the liquid absorption speed of ECM-based powders is significantly better than the representative hemostatic powder such as Celox™, Zeolite and Yunnan Baiyao powder (YB). It is worth noting that Celox™ did not absorb liquid obviously at 5 s. Large specific surface area and natural hydrophilicity of ECM-based powders are conducive to the rapid penetration of the liquid. We further evaluated the liquid absorption capacity of the powders, demonstrating the similar results that AP, APS, and APSO powders could absorb approximately 8 times their own weight in liquid within 5 s (Fig. 1e). This may be due to the comparable morphology and hydrophilic properties. Notably, this excellent performance is independent of liquid environments whether phosphate buffer saline (PBS) or anticoagulant blood. Depicted in Fig. S5 in Supporting Information, the liquid absorption ratio of 30 s is very close to that of 5 s, meaning the ECM-based powders completely attained a stable state just for 5 s.

The self-assembly characteristics of ECM-based powders were visually displayed in Fig. 1f and Movie S1 in Supporting Information. The self-assembly of APSO powder occurred within 5 s after absorbing liquid, presenting a gel-like structure. Additionally, it could quickly form a tight barrier to obstruct blood flow after turning the tube, and, in sharp contrast, the Celox™, YB and Zeolite powders without self-assembly ability failed to this (Fig. 1g and S6, Movie S2 in Supporting Information). As revealed by X-ray photoelectron spectroscopy (XPS) and FTIR results (Fig. S7 in Supporting Information), multiple covalent interactions (borate ester bonds and Schiff base bonds) and non-covalent interaction (hydrogen bonds) were formed in the APSO hydrogel after self-assembly. The hydrogen bonds were further demonstrated by rheological tests. We used the disruption of hydrogen bonds by urea to verify the role of hydrogen bonds in hydrogels [34]. In Fig. S8 in Supporting Information, as the concentration of urea in hydrogel increased from 0 to 40 mM, the G' decreased from 3944 Pa to 1002 Pa, indicating that hydrogen bonding plays an important role in the formation of the hydrogel network.

Moreover, the self-assembly time of reported self-assembly powders was comprehensively compared in Fig. S9 in Supporting Information, it can be seen that APSO powder exhibits significant superiority in hydrogels composed of natural and composite polymers. Moreover, of note, anticoagulant blood have no influence on self-assembly process, which is favor of the application in complex scenarios, such as patients with coagulopathy and cardiovascular surgery [35].

2.2. Characteristics of self-assembled ECM-based hydrogels

Initially, to ensure the uniform property of the hydrogel formed by the powder, the preparation of ECM-based hydrogels was strictly controlled. According to the previous results, AP, APS and APSO hydrogels were prepared after the corresponding powder have absorbed the liquid for 5 s. The structure, stability and rheology properties of self-assembled ECM-based hydrogels were evaluated systematically.

By observing the cross-sectional morphology after lyophilization, we found that all ECM-based hydrogels have typical porous structure and no obvious particles exist, proving the complete self-assembly (Fig. S10, Supporting Information). As a symbol of crosslinking extent in hydrogel network, the average pore size of APSO hydrogel (36.12 ± 7.74 μm) was significantly smaller than the AP and APS hydrogels (55.74 ± 12.50 μm and 45.77 ± 9.53 μm, respectively) listing in Fig. 2a. The swelling and degradation behaviors of hydrogel were conducted to evaluate its stability. The swelling equilibrium time (T_{SE}) of APSO hydrogel was about 24 h with the swelling rate of 69.09 ± 16.16 %. The T_{SE} of AP and APSO was about 48 h, and the swelling rates of them were 1.72 and 1.34 times that of APSO hydrogel respectively (Fig. 2b). In the hemostasis, the swelling rate of hydrogel should be moderate. On the one hand, excessive swelling ratio may weaken its mechanical properties and bioadhesion ability; On the other hand, for soft tissues such as liver, brain and nerves, excessive swelling ratio may produce pressure and cause unnecessary trouble [36]. Similarly, APSO hydrogel degraded more slowly than the other two materials. Importantly, all ECM-based hydrogels can be completely degraded within a month, which is benefit for the *in vivo* application. Overall, APSO hydrogel exhibited the tightest microstructure and the best stability, ascribed to the formation of more binding sites between SIS-OH and ADA-PBA.

The rheology was used to evaluate the viscoelasticity, one of the imperative properties of hydrogels. Fig. 2d showed that the rheological behavior of AP, APS and APSO hydrogels present the similar change under the increasing frequency. The failure frequency when storage modulus (G') less than loss modulus (G'') of AP hydrogel was 72.6 Hz, whereas the other two hydrogels remain intact (G'>G'') even reaching the testing maximum (100 Hz). Among them, giving the credit to SIS and SIS-OH into the hydrogel system, more hydrogen bonds could sacrifice to dissipate external energy [37].

As depicted in Fig. 2e, the rheological property of AP, APS and APSO hydrogels showed gel-like characteristic and be basically constant at 1–10 % strain, where the G' of the APSO hydrogel was 5157 Pa, approximately 2.21 and 1.82 times those of the AP and APS hydrogels, profited from the covalent/non-covalent interactions (i.e., Schiff bases, borates, hydrogen bonds) in hydrogel networks. As the strain increases further, all hydrogels fail at 47.2 % strain. Consequently, the formed hydrogel can meet the application in the body without being destroyed, which the maximum strain *in vivo* does not exceed 10 % as reported [38]. Using alternate step strain sweep mode in Fig. 2f, the self-healing property of hydrogels was verified, enable to rebuild and restore to the original modulus after destruction of high strain (300 %). As shown in Fig. S11 in Supporting Information, followed by touching each other, two dyed APSO hydrogels could be picked up with the tweezer and further stretched without breaking, indicating the satisfactory self-healing property. This endow the hydrogel the ability to withstand

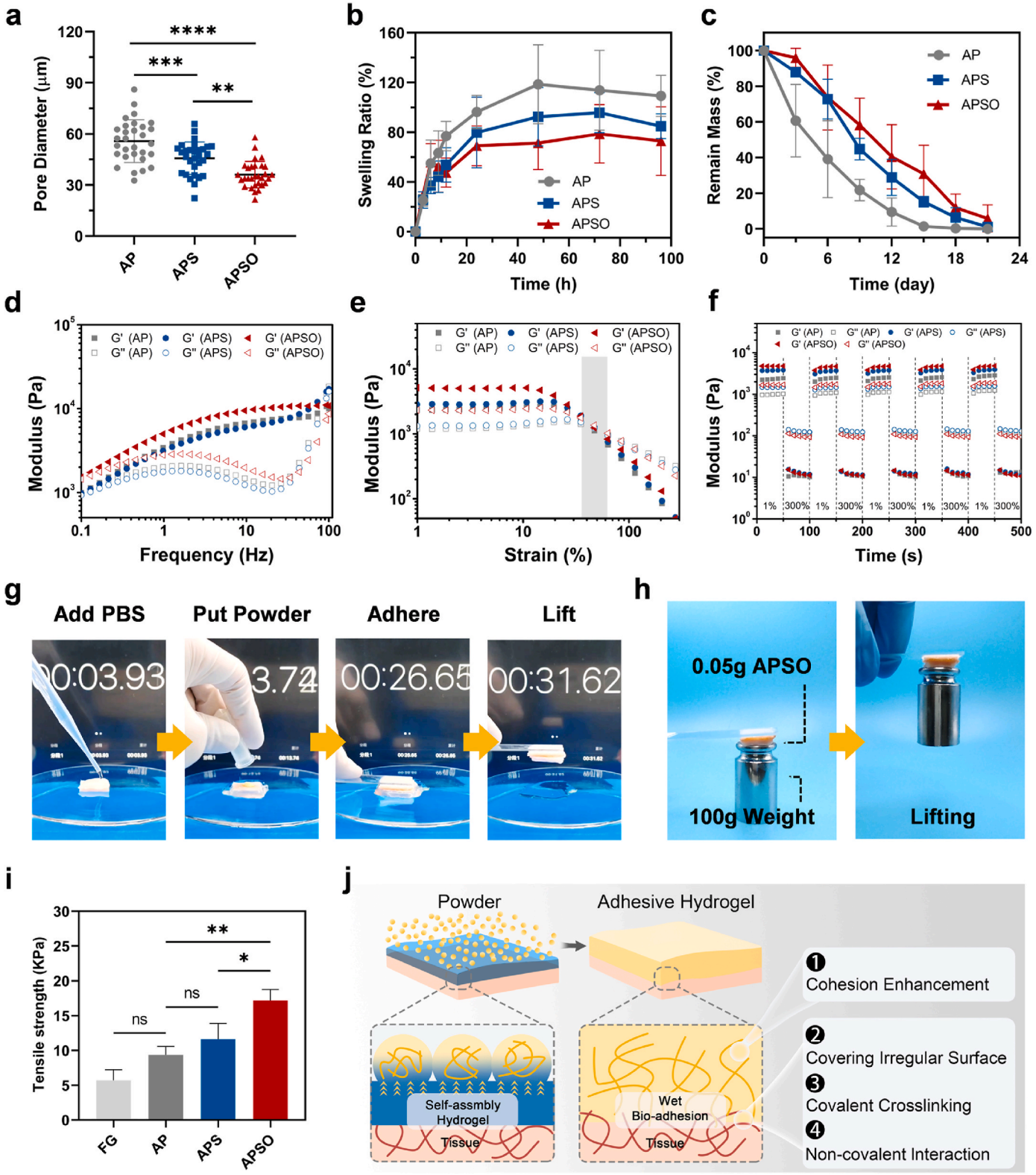

Fig. 2. a) The pore diameter of the AP, APS, and APSO hydrogel (n = 30); b) The swelling curves and c) degradation curves of the different hydrogels; The rheological curves of the AP, APS, and APSO hydrogels under d) frequency sweep mode, e) strain amplitude sweep mode and f) alternate step strain sweep mode (low strain: 1 %, high strain: 300 %); g) Wet bio-adhesion of the APSO with a wet pigskin in a short time; h) The evaluation of bio-adhesion that using APSO powders (0.05 g) to lift the weight (100 g); i) The tensile strength (KPa) of commercial fibrin glue (FG), AP, APS, and APSO powders; j) The wet bio-adhesion mechanism of APSO powders: interfacial liquid removing, instant self-assembly, and enhanced bio-adhesion based on multiple mechanisms. (*$P < 0.05$, **$P < 0.01$, ***$P < 0.001$, ****$P < 0.0001$, *ns*: no significant difference).

the external pressure and maintain complete barrier, even if damaged by high-speed blood flow. Reversible covalent bonds (i.e., borate ester and Schiff base bonds) and non-covalent interaction in hydrogels significantly contribute to enhance self-healing [39]. Notably, self-healing behavior is also one of the pivotal mechanisms for instant self-assembly of ECM-based powders.

2.3. Wet bio-adhesion and its mechanism

Considering the wet environment caused by bleeding, the importance of tissue wet bio-adhesion in the hemostasis has been gradually recognized [10]. The wet bio-adhesion of ECM-based powders was firstly examined using wet pigskin. Upon pouring APSO powder, the surficial liquid absorption swiftly occurred, enabling the pigskin to be adhered and lifted with another one within 5 s (Fig. 2g and Movie S3, Supporting Information). And 0.05 g of APSO powder was employed to bond two wet pigskins together, which subsequently demonstrated remarkable wet bio-adhesion by lifting a weight that was 2000 times its own mass (Fig. 2h and Movie S4, Supporting Information). The SEM images in Fig. S12 in Supporting Information showed that the hydrogel closely adhered to the pig skin without separation. Furthermore, tensile test using universal testing machine was also employed to evaluate the bio-adhesion of ECM-based powders (Fig. S13, Supporting Information). Here, clinically applied fibrin glue (FG) was selected for comparison [40]. As illustrated in Fig. 2i, the AP, APS and APSO powders showed great bio-adhesion, and, among them, the tensile strength of APSO powder (17.18 ± 1.57 KPa) is the most prominent, reaching 3.00 times of FG (5.72 ± 1.51 KPa) ($P = 0.0001$). In addition, the wet adhesion of the powder and prefabricated hydrogel was tested. As shown in Fig. S14 in Supporting Information, the tensile strength of prefabricated APSO hydrogel is 4.2 ± 6.0 KPa, which was only 23 % of the tensile strength of APSO powder. This is because the persistence of interfacial water severely affects bio-adhesion. This implies that the self-assembly strategy is essential for wet bio-adhesion, to some extent contributing to the prevention of adhesion after hemostasis.

Furthermore, a bursting test was used to further evaluate the tissue sealing ability. In Fig. S15 in Supporting Information, the burst pressure of self-assembled APSO hydrogel (141.00 ± 12.13 mmHg) was significantly higher than that of the fibrin glue (FG), AP and APS hydrogels, which may be attributed to the superior cohesion and adhesion strength of the APSO hydrogel. Notably, this value was significantly higher than the normal human blood pressure of 120 mmHg, thereby making it a promising sealing agent for hemostasis [6].

Through in-depth analysis of its wet bio-adhesion mechanism, we believe that this is the synergistic effect of multiple factors (Fig. 2j). The wet bio-adhesion process could be divided into two steps. For the first, the bleeding area is a complex environment with flowing blood and irregular appearance. The presence of interfacial blood poses an apparent barrier to bio-adhesion, particularly in non-compressible organs. The small ECM-based powders are highly appropriate for covering irregular morphology, and the exceptional liquid absorption capacity allows for rapid absorption of blood, thereby establishing the groundwork for bio-adhesion. It is worth mentioning that liquid absorption is the precondition of the following process, necessitating the interfacial water as an indispensable factor to initiate the self-assembly.

As to second step, the self-assembly instantly completed within 5 s, forming a stable physical barrier to seal wound in situ. Importantly, there involves three distinct adhesion mechanisms. For the hydrogel, the cohesion enhancement could significantly ameliorate the bio-adhesion properties of the hydrogel [41]. Compared with the other two, the multiple crosslinking mechanisms in APSO hydrogel render the higher molecular network density and mechanical properties, capable of resistant to external stress and achieving cohesion-adhesion balance. For the hydrogel-tissue interface, the small size of the ECM powder facilitates rapid coverage of irregular wounds. Furthermore, many intrinsically adhesive groups (such as hydroxyl, aldehyde, and benzene rings) in hydrogels could induce various covalent/non-covalent interactions. Taken together, contributing to the above comprehensive mechanisms, APSO powder has the best wet bio-adhesion capacity, critical for rapid wound closure and effective hemostasis.

2.4. Biocompatibility and cell recruitment bioactivity

The satisfactory biocompatibility is a prerequisite for safe and effective clinical application of biomaterials [42]. For cytocompatibility, the effect of ECM-based hydrogel on the cell proliferation and activity was verified by CCK-8 assay and live/dead staining assay, respectively. Fig. 3a showed live/dead staining images of HUVECs after 1 and 3 days of incubation with AP, APS and APSO hydrogels. The cells maintained paving stone-like morphology, and proliferated normally with minimal cell death. Furthermore, the proliferation of HUVECs stimulated by ECM-based hydrogels was not significantly different from that of the control group (Fig. 3b). Besides, in Fig. S16 in Supporting Information, the BMSCs and NIH-3T3 treated with the AP, APS and APSO hydrogels also exhibited the outstanding cell activity and proliferation, further confirming the reliable compatibility. The hemolysis test is the gold standard used to judge hemocompatibility [43]. After incubation the erythrocyte suspension with ECM-based hydrogel, few cell rupture occurred, and the hemolysis rate of AP, APS, and APSO hydrogels were all lower than 5 %, with 3.23 ± 0.70 %, 2.55 ± 0.72 % and 2.64 ± 0.81 %, respectively, demonstrating reassuring hemocompatibility (Fig. 3c). Histocompatibility is also important for the evaluation of biocompatibility, which reflect the reaction between the implant and the host. The APSO hydrogel was embedded subcutaneously in rats for 1 and 2 weeks. As shown in Fig. S17a, no tissue necrosis, hyperemia and purulency were noticed in the subcutaneously implanted area, and the material volume was significantly reduced over time, denoting their biodegradability *in vivo*. To further investigate the inflammatory response of material *in vivo*, the iNOS, M1-type macrophage marker, surrounding the implanted area was evaluated [29]. As shown in Figs. S17b and c, the $iNOS^+$ area is mainly concentrated around the implant, signifying the normal inflammatory response of the body used to remove foreign bodies. As the material degraded, the $iNOS^+$ area exhibited a significant reduction. Specifically, after 2 weeks of implantation, the $iNOS^+$ area decreased to 23.80 % of that in 1 week ($P = 0.0139$), which indicated the diminished inflammatory response and excellent histocompatibility of the APSO hydrogel. All of the above indicate that hydrogels have excellent biocompatibility.

The cell recruitment of ECM-based hydrogels was firstly evaluated by a Transwell migration assay (Fig. 3d, e and S18). After 24 h incubation, the three kinds of cells in the lower chamber of all ECM-based hydrogel groups were significantly more than those in the control group. Moreover, this boosting effect was further amplified when hydrogels contained SIS component, that the cells per field of HUVECs in APS and APSO groups was 1.60 and 1.54 times that of AP hydrogel, which proved that SIS can release relevant biological cues to promote cell recruitment. We also proved this point through scratch experiments, and the result showed that HUVECs were able to migrate more quickly in response to ECM-based hydrogels. The migration rate of AP, APS and APSO hydrogels reached 79.47 ± 2.63 %, 92.68 ± 3.01 % and 87.80 ± 5.69 % respectively at 48 h, while that of the control group was only 59.54 ± 7.43 % (Fig. 3f and g). Cell recruitment in ECM-based hydrogels is very beneficial to accelerate the process of wound repair.

2.5. Neovascularization and enhanced endothelial cell functions bioactivity

The ability to promote angiogenesis is critical for tissue regeneration, which facilitates substance delivery, intercellular signaling, recruitment of endogenous stem/progenitor cells, etc [44]. Tube formation assay results showed that, after stimulation by APS and APSO hydrogels, HUVECs quickly formed tubular structure and interconnected network,

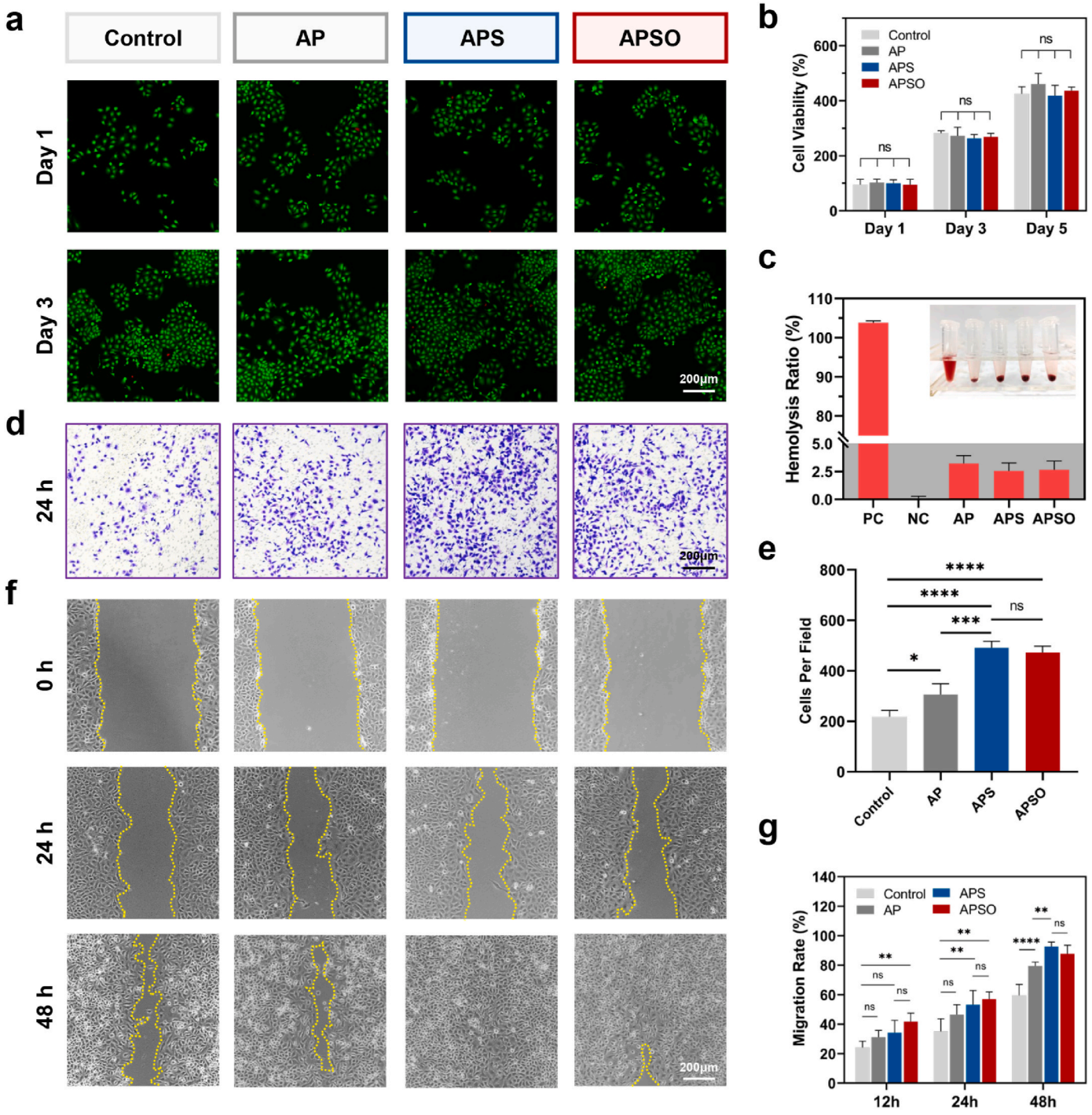

Fig. 3. a) Live/Dead staining images and b) CCK-8 assay after incubation HUVECs with AP, APS and APSO hydrogel; c) Hemolysis ratio (%) of AP, APS and APSO (PC: 0.1 % Triton X-100, NC: PBS); d) The images and e) cells per field in Transwell migration assay of HUVECs treated with hydrogels; f) The images and g) migration rate (%) of HUVECs treated with the different hydrogels in scratch test. (*$P < 0.05$, **$P < 0.01$, ***$P < 0.001$, ****$P < 0.0001$, *ns*: no significant difference).

revealing the pro-angiogenesis of ECM-based hydrogels (Fig. 4a). Additionally, significant increases in both total length and number of meshes were further confirmed in the APS and APSO group, but not in the AP group (Fig. 4b and c).

Dense and healthy endothelium can play an active role in vascular wall remodeling, and healthy endothelial cells have an antithrombotic effect *in vivo* by releasing substances such as nitric oxide (NO) and prostaglandin-I-2 (PGI_2) [45]. The NO in AP, APS and APSO-incubated HUVECs were successfully labelled using a fluorescent probe, DAF-FM DA. And the fluorescence intensity of AP, APS and APSO groups was 122.12 ± 21.98 %, 195.14 ± 28.98 % and 180.70 ± 36.00 % of the control group, respectively (Fig. 4d and S19, Supporting Information). Moreover, as indicated by Fig. S20 in Supporting Information, the PGI_2 release level possessed a significant improvement in APSO-incubated HUVECs with being of 224.68 ± 8.62 pg mL^{-1}, 1.38, 1.15 and 1.05 times that of control, AP and APS groups. These functional evaluations illustrated the excellent endothelial cell function enhancement of ECM-based hydrogels.

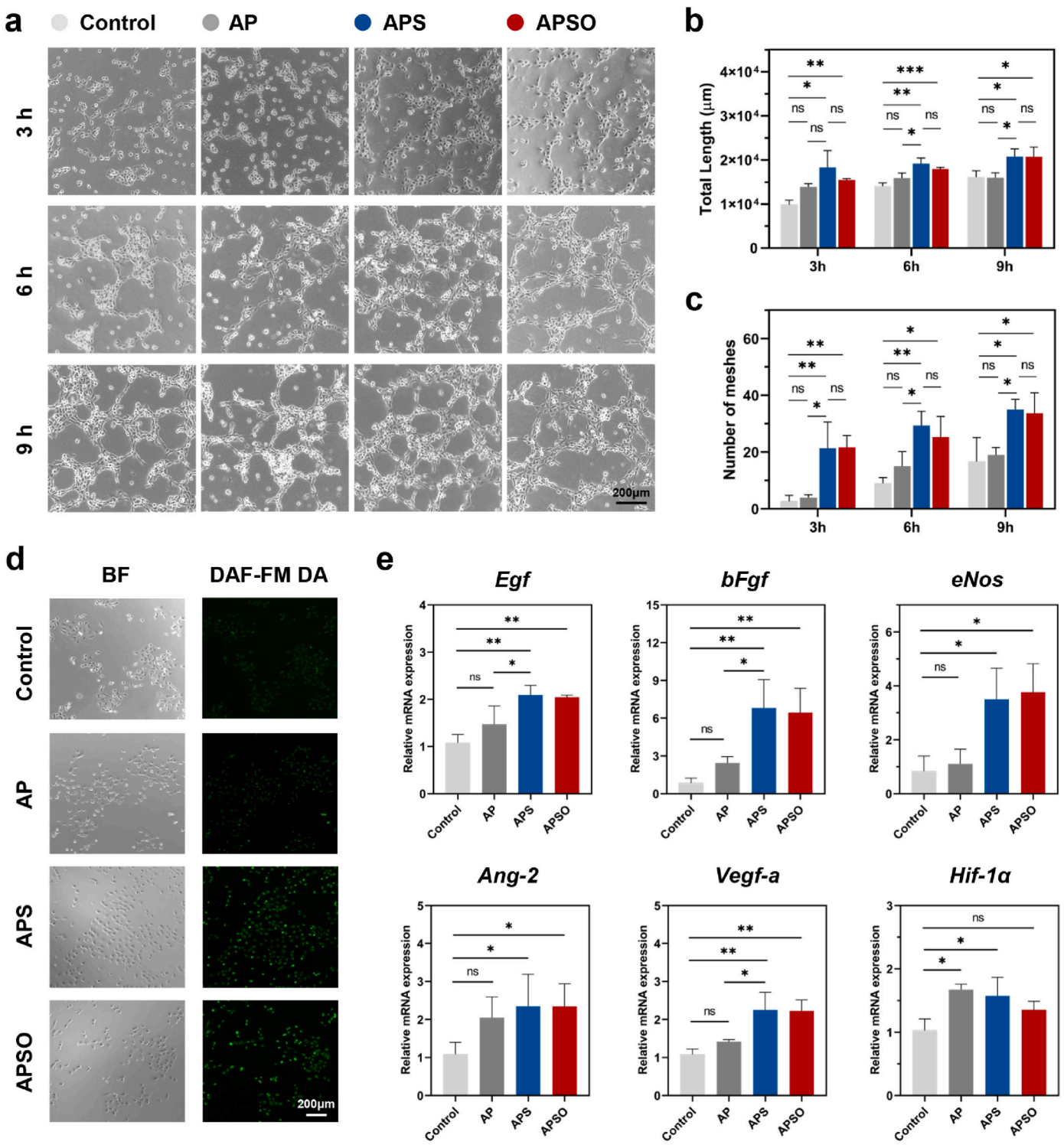

Fig. 4. a) Images and statistical analyses of b) total length (μm) and c) number of meshes in tube formation assay of HUVECs treated with AP, APS and APSO hydrogels; d) The bright field (BF) and fluorescent images stained with NO fluorescent probe (DAF-FM DA) of HUVECs treated with AP, APS and APSO hydrogels; e) Expression of the representative angiogenesis and endothelial cell function-related genes in HUVECs after treatment of different hydrogels evaluated by RT-qPCR. (*$P < 0.05$, **$P < 0.01$, ***$P < 0.001$, *ns*: no significant difference).

Finally, the expression levels of genes associated with angiogenesis and functions in endothelial cells were detected by real-time quantitative polymerasechain reaction (RT-qPCR) (Fig. 4e). The results showed that APS and APSO hydrogels could upregulate the expression levels of *Egf*, *bFgf*, *eNos*, *Ang-2*, *Vegf-a* and *Hif-1α* in HUVECs compared with the control and AP groups. Among them, eNOS mainly regulates the synthesis of NO in vascular endothelium, which is an important factor in regulating vascular endothelial function. EGF and bFGF are vital in promote the proliferation, migration and morphological maintenance of endothelial cells, eNOS and Ang-2 mainly regulates the synthesis of NO and endothelial cell homeostasis [46]. VEGF, as a specific mitogen of vascular endothelial cells, significantly ameliorates endothelial cell proliferation, meanwhile involved in multiple signaling pathways such as *Hif-1α/Vegf-α* to induce angiogenesis [47]. As previously reported,

our results also provide further evidence of the significant angiogenic capacity of SIS, which is not affected by moderate hydroxylation [27]. In addition, hemostatic materials and their degradation products are often concerned about local/systemic thrombosis *in vivo* due to their coagulation function. Hence, from this point of view, the endothelial cell function strengthening of ECM-based hydrogels is conducive to solving this problem.

2.6. Hemostatic application of the ECM-based powders

The hemostatic effect of ECM-based hydrogels was evaluated using the model of non-compressible hemorrhage in rabbit liver volume defect shown in Fig. 5a. The liver was chosen because of its abundant blood supply and high fragility. As seen in hemostatic process (Fig. 5b and Movie S5, Supporting Information), without any treatment, the damaged liver continued to bleed, reaching a blood loss of 3.23 ± 0.55 g in 5 min. In stark contrast, upon the application of the ECM-based powders, the severe hemorrhage was promptly halted. Once contacting blood, APSO powder absorbed it followed by ultrafast self-assembly, forming a physical barrier with strong wet adhesion ability. The blood loss in APSO group was 0.78 ± 0.22 g, which was respectively reduced by 76 % and 60 % compared with control and Celox™ groups, proving the excellent ability to hemostasis (Fig. 5c). APSO group also has less blood loss than AP and APS groups due to its superior wet bio-adhesion.

Aiming to further investigate the effect of the material on the hemostatic process, the bleeding site after the application of APSO powders was observed by SEM. According to the typical morphology, the viewing area was segmented into outer, middle and inner layers, as shown in Fig. 5d and e. In the outer layer, the apparently dense and sturdy network of fibers has emerged, enveloping many erythrocytes. This demonstrated the successful self-assembly of ECM-based powder in the blood, and a substantial quantity of fibrin networks intricately intertwine with hydrogel networks, thereby constructing a robust physical barrier (Fig. 5f); In the middle layer, a tangled and loose fibrous structure dominated by fibrin network means that the formation of a lot of blood clots, which is caused by a strong external physical barrier that prevents the flow of blood (Fig. 5g); In the inner layer, the erythrocytes morphology changed greatly, showing an irregular polyhedron. This could be due to the contraction stress generated by the stretching and bending of fibrin networks, and the trapped erythrocytes are forced to aggregate and deform [48]. This change facilitates the creation of an impermeable barrier between the material and the bleeding tissue (Fig. 5h). Concurrently, Hematein and Eosin (H&E) staining was employed to observe the bleeding site (Fig. S21 in Supporting Information). Similar to SEM results, APSO powder self-assembled to seal the bleeding site, and the blood clots containing many erythrocytes and fibrin networks formed inside.

Furthermore, massive hemorrhage models were constructed on the rabbit heart and femoral artery (Fig. 6a). Under high blood pressure and dynamic condition, APSO powder can still function wet bio-adhesion on heart surface to control bleeding, which also confirmed by H&E staining after hemostasis (Fig. 6b and c and Movies S6-7, Supporting Information). However, Celox™ powder failed to stop heart hemorrhage due to its lack of rapid liquid absorption and wet bio-adhesion (Fig. S22, Supporting Information). When faced with cylindrical femoral arteries, APSO hydrogel could completely seal the wound, showing a reliable hemostatic effect (Fig. 6d and e and Movie S8, Supporting Information), Here, the blood loss in APSO group (0.26 ± 0.15 g) was almost negligible compared with the blank (14.55 ± 4.33 g) ($P = 0.0024$) (Fig. 6f and g). In short, ECM-based powders, especially APSO powder, could quickly seal wound and showed excellent hemostatic ability for non-compressible and massive hemorrhage.

5

The three ECM-based hemostatic powders are able to efficiently absorb liquids due to the high hydrophilicity of their components. Meanwhile, effective tissue sealing should be emphasized in the application of hemostasis. For APSO powder, the stability, adhesion strength and mechanical properties are outstanding, especially the ability to withstand arterial blood pressure, which is essential for its control of massive and non-compressible hemorrhage. The bioactivity of the material is a key consideration in the process of tissue repair after hemostasis. APSO powder have no difference with APS in promoting cell migration, angiogenesis and endothelial function, indicating that mild modification of SIS did not affect its bioactivity. Among the three ECM-based hemostatic powders, APSO powder demonstrates superior performance in the development of hemostatic materials integrating hemostasis and tissue repair. Consequently, it was selected for further *in vivo* tissue repair experiments.

2.7. In vivo biodegradation of ECM-based powders

In clinical applications, hemostatic materials that can safely biodegrade *in vivo* and promote tissue repair will greatly benefit doctors and patients [49,50]. Hence, we further systematically evaluated whether APSO powder can meet all-in-one needs. Consistent with the above, the model of non-compressible bleeding in rabbit liver volume defect was constructed for in-situ tissue repair evaluation after hemostasis. Here, electrosurgery unit hemostasis, the most commonly used method in the clinic, was set as the control group (ESU group). Macroscopic observation revealed that the liver after hemostasis using APSO powder showed the superior wound healing, the defected site was basically the neonatal liver (Fig. S23, Supporting Information). Depicted in Fig. 7a, many cell infiltration occurred in APSO group 14 days after surgery, which is a normal immune response of the body and is conducive to the materials degradation. Moreover, capsule layer and tissue lesions have not occurred, indicating the good biocompatibility of APSO powder. After day 28, it was basically degraded completely, and the tissue in repaired area had a similar structure to normal liver. A little fiber tissue on the liver surface may be the adhesion with the abdominal wall. Nevertheless, in the ESU group, in addition to unabsorbed blood clots, numerous fibrous structures were present 14 days after surgery, and this phenomenon did not change over time. Sirius red staining was used to observe collagen deposition in the repair area (Fig. 7b and c). As in normal liver (2.10 ± 0.03 %), the APSO group have no additional collagen deposition (2.40 ± 0.53 %), while the ESU group was an alarming 45.64 ± 3.67 %.

At the same time, blood samples were collected at 14 and 28 days postoperatively to determine the systemic toxicity of the degradation products on the body (Fig. 7d and e). There was no significant statistical difference between all indicators among normal, APSO (Day 14), and APSO (Day 28) groups ($P > 0.05$). No distinct changes in blood cells, suggesting that no abnormal response in inflammatory responses and coagulation function. In brief, the above results indicated that APSO powder could safely biodegraded *in vivo*, and the degradation products will not cause serious foreign body reactions.

2.8. In-situ liver functional repair after hemostasis of ECM-based powders

Blood vessels and bile ducts are key structures in the liver and are considered markers of functional liver regeneration [51]. The endothelial cells of vascular and bile duct were stained by immunohistochemical staining (IHC) of CD31 and CK19, respectively. As listed in Fig. 8a and b, the typical structure of hepatic sinusoid were observed in the APSO group for 28 days, while connective tissue occupied the repair area in the ESU group. The integrated option density (IOD) of CD31 in APSO group is 83.73 ± 6.65 % of the normal group ($P > 0.05$). Similarly, bile ducts were observed in the portal triad of APSO group, a structure that plays an important role in the microcirculation of the liver (Fig. 8c). The CK19 relative IOD of the APSO and ESU groups was respectively 85.81 ± 11.14 % and 28.99 ± 12.54 % of the normal group, meaning a large difference in repair effect (Fig. 8d). These results showed that the basic reconstruction of microcirculation network in APSO group,

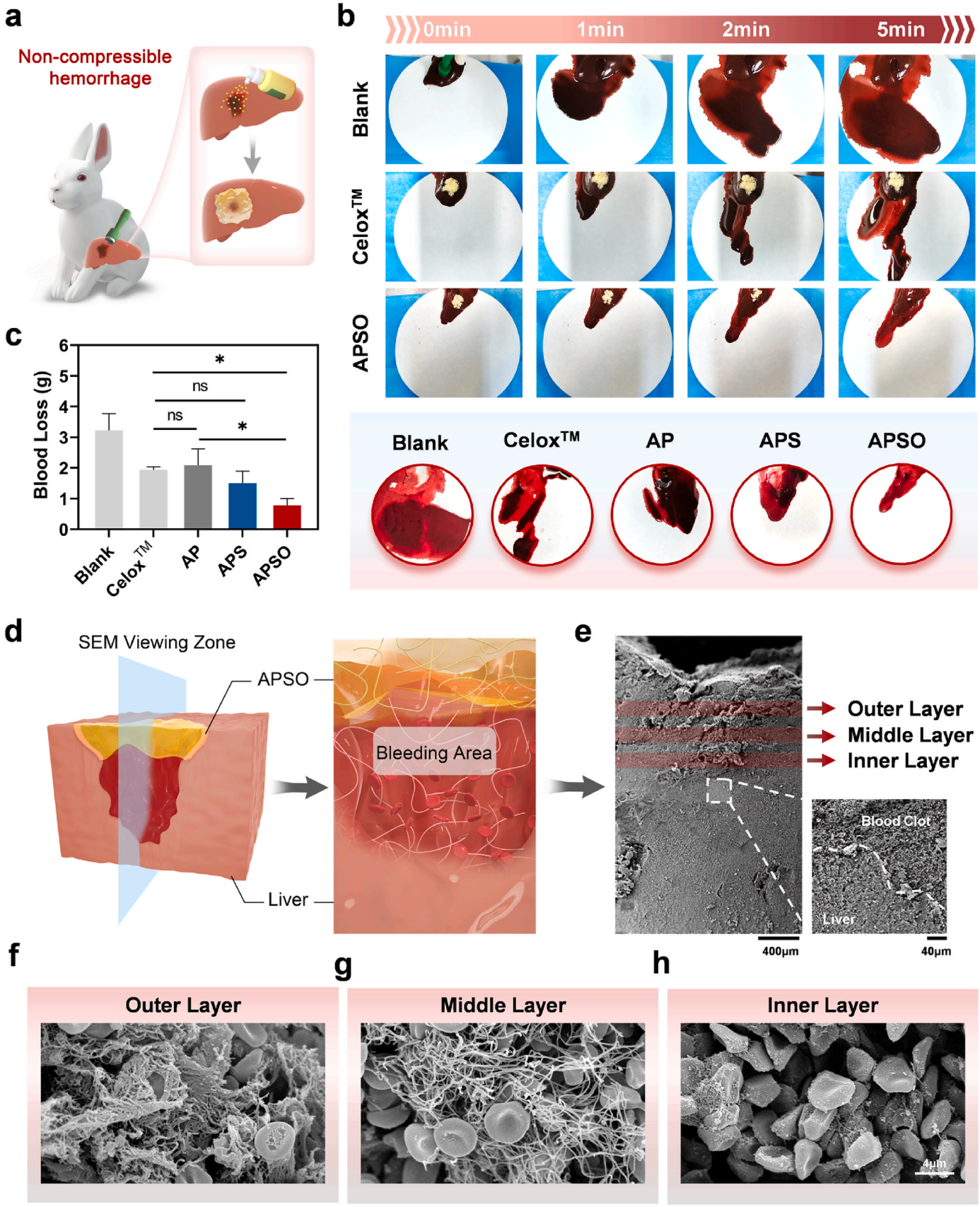

Fig. 5. a) The scheme of non-compressible hemorrhage in rabbit liver volume defect and application of APSO powders; b) The hemostatic process in blank group (i.e., no treatment), Celox™ and APSO groups, and the images of filter paper after hemostasis; c) The blood loss (g) after different treatments; d) The SEM viewing zone scheme and e) SEM images of the liver bleeding site; SEM images of corresponding f) outer, g) middle and h) inner layers. (*$P < 0.05$, ***$P < 0.001$, ****$P < 0.0001$, *ns*: no significant difference).

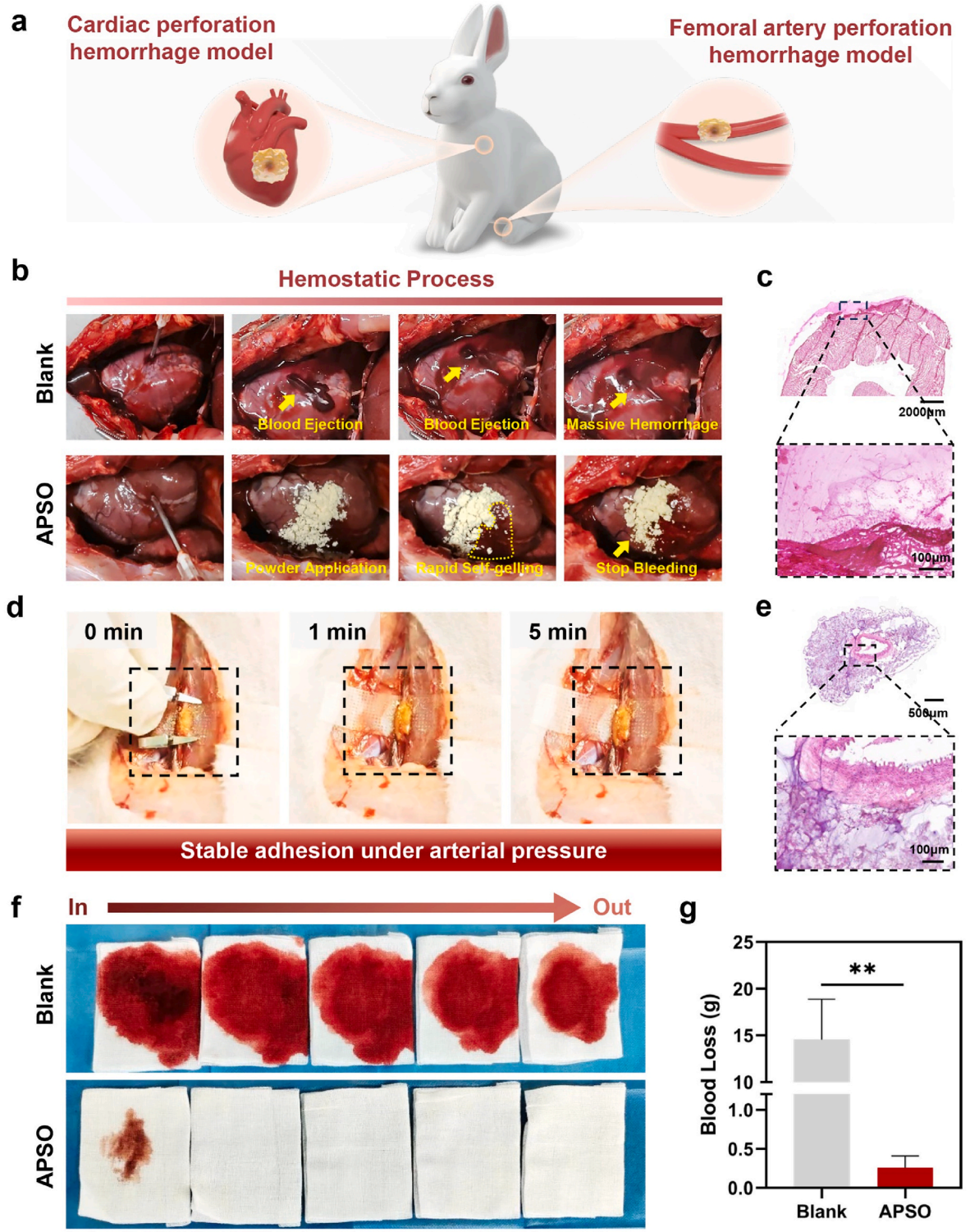

Fig. 6. a) The scheme of rabbit massive hemorrhage models and application of APSO powders; b) The hemostatic process in blank group (i.e., no treatment) and APSO group in rabbit cardiac perforation massive hemorrhage model, and the corresponding c) H&E staining images of cardiac surface adhered to hydrogel; d) The images of APSO hydrogel tightly sealed the bleeding rabbit femoral artery and the corresponding e) H&E staining images; f) Bleeding situation and g) blood loss (g) of blank and APSO groups in rabbit femoral artery perforation massive hemorrhage model. (**$P < 0.01$).

conducive to the rapid absorption of material degradation products.

Moreover, glycogen production, representing the important hepatocytes function, was evaluated by Periodic Acid-Schiff (PAS) staining [52]. The hepatic lobules in the repair area of APSO group were obviously stained, and the positive area was 70.83 ± 8.56 % of the normal group, significantly higher than that in the ESU group (4.57 ± 2.99 %, $P = 0.0048$) (Fig. 8e and f). Key indicators related to protein synthesis (TP and ALB) and liver damage (AST and ALT) were further examined. The results in Fig. 8g showed no significant difference between the APSO group and the normal group ($P > 0.05$), indicating that APSO powder can promote functional liver repair. However, the ESU group showed obvious liver damage, that ALT and AST showed significant difference

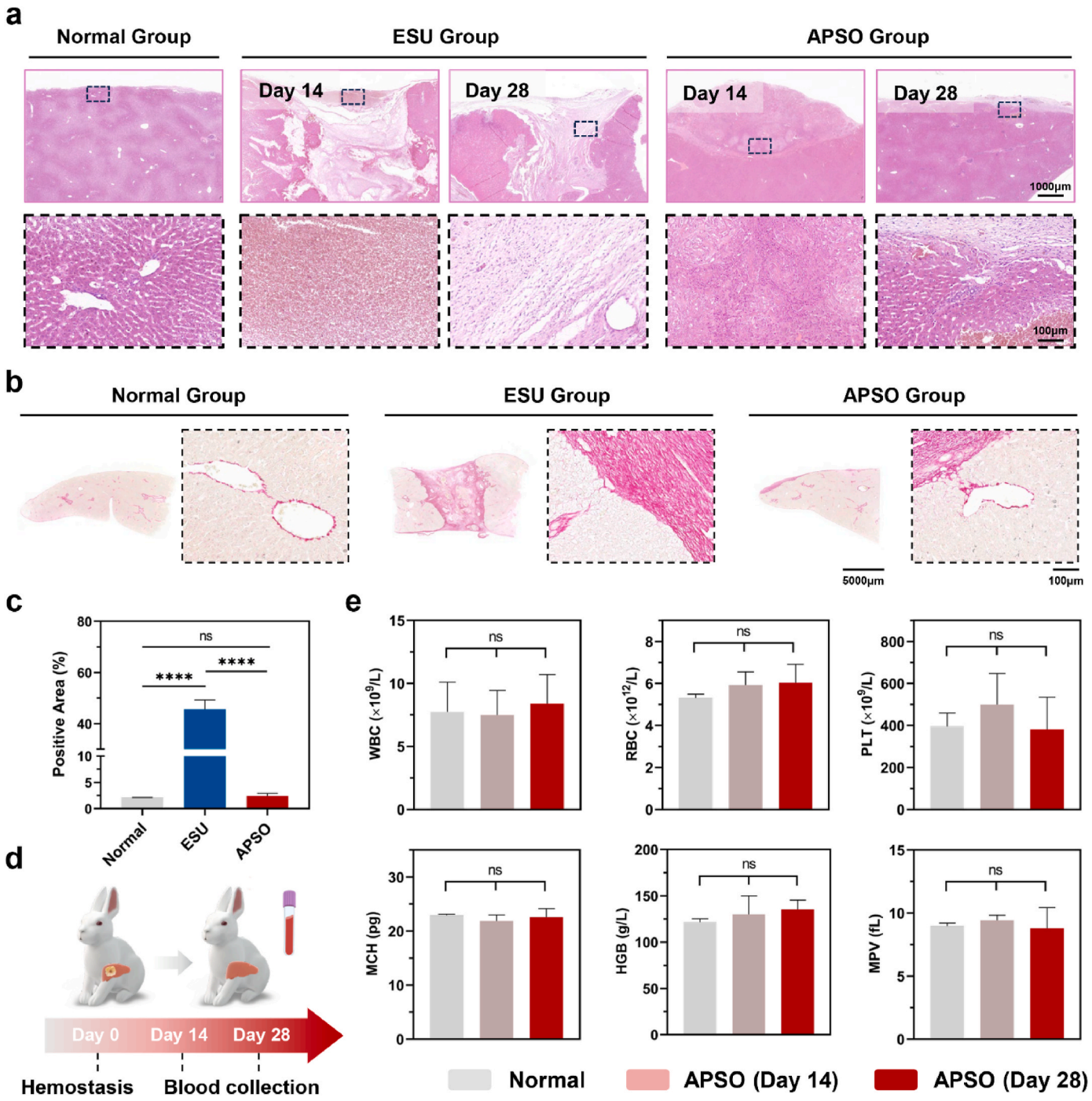

Fig. 7. a) H&E staining of liver bleeding site at day 14 and 28 postoperatively treated by ESU (electrosurgery unit) and APSO powder (normal group, health liver tissue); b) Sirius red staining images and c) positive area (%) of different groups at day 28; d) Schematic diagram and e) results of rabbits blood routine tests during tissue repair. (****$P < 0.0001$, *ns*: no significant difference).

compared with normal group. From these results, we could see that although ESU is widely used for hemostasis, due to its thermal damage, the impaired tissue cannot regenerate functionally, especially for large area defects. All-in-one APSO powder can not only control bleeding quickly, but also induce tissue repair in situ (Fig. 8h). The mechanisms were summarized: Firstly, the bio-adhesive APSO hydrogel provides a reliable physical barrier after hemostasis and keep the wound area moist, conducive to promote tissue repair [20,53]. Notably, the self-gelling process is initiated by blood, leading to the intertwining of molecular networks between the hydrogel and the blood clot. Simultaneously, cellular components such as platelets and erythrocytes become entrapped. As reported, blood clots can induce immune niche formation by recruiting and activating various immune cells, which in turn further promote the material degradation and the release of inherent biological cues [54–56]. The molecular mechanisms underlying the interaction between the APSO hydrogel and immune cells will be further elucidated in future studies; Secondly, the versatile bioactivities contained in ECM rapidly induce the neovascularization and enhanced endothelial cell functions, accelerating the formation of blood vessels and bile ducts; Finally, the reinforced substance transport capacity promoted the complete materials biodegradation and induced neonatal tissues, and achieved functional regeneration of the liver.

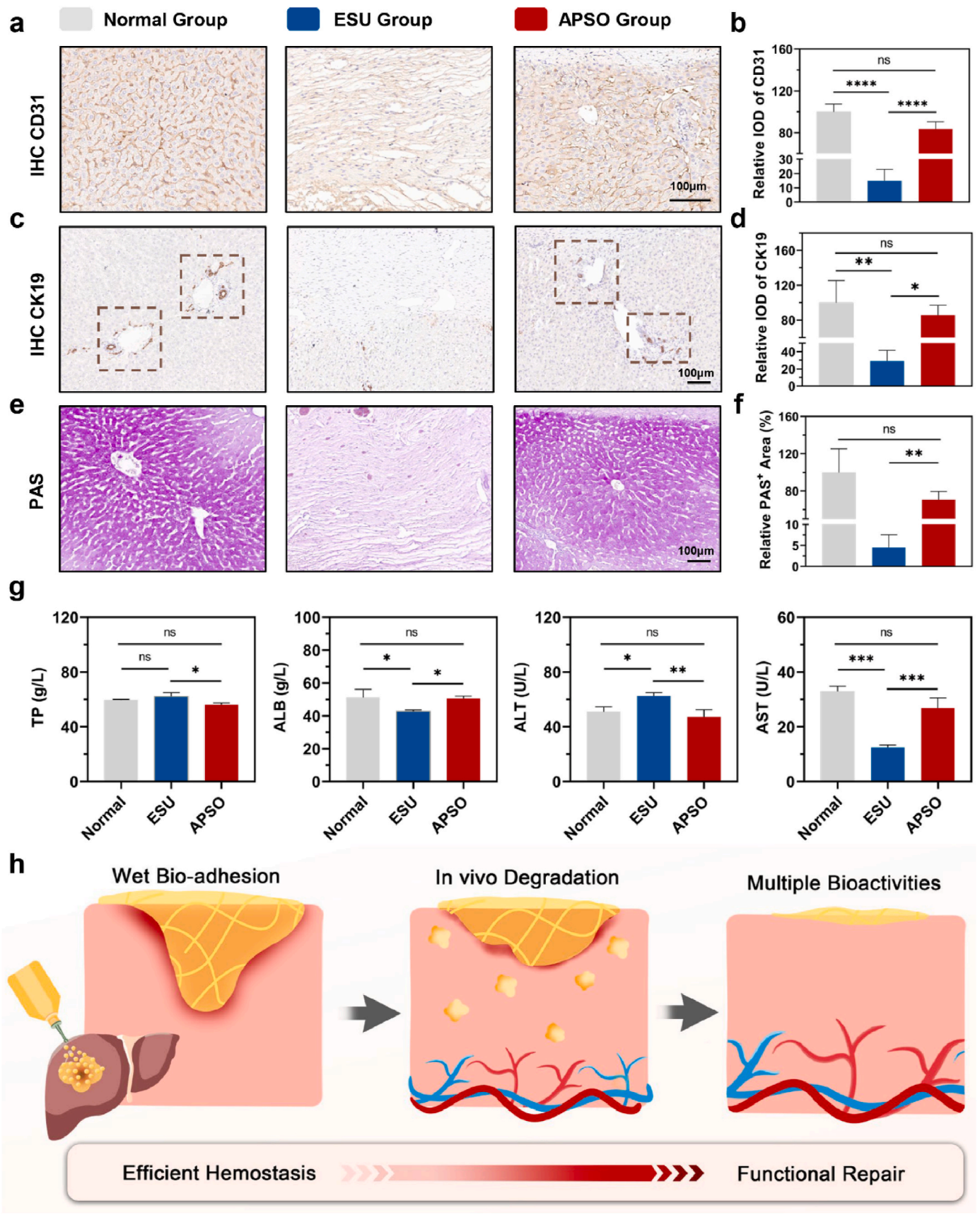

Fig. 8. a) CD31 IHC staining and b) quantitative analysis of liver repair area in normal, ESU and APSO groups at day 28; c) CK19 IHC staining and d) quantitative analysis of liver repair area in all groups at day 28; e) Periodic Acid-Schiff (PAS) staining and f) relative PAS^{+} area of liver repair area in all groups at day 28; g) Evaluation of liver function at day 28; h) Schematic diagram of ECM-based powder safely biodegraded *in vivo* and in situ induced tissue functional repair after hemostasis. (*$P < 0.05$, **$P < 0.01$, ***$P < 0.001$, ****$P < 0.0001$, *ns*: no significant difference).

3. Conclusion

In this study, we prepared all-in-one ECM-based powders aimed at achieving efficient hemostasis while facilitating in situ tissue functional repair. Utilizing the inherent hydrophilicity and multi-crosslinking strategy of materials, the ECM-based powders demonstrate liquid absorption and ultrafast self-assembly within 5 s, forming a hydrogel with excellent wet bio-adhesion. This effectively integrates the advantages of both powder- and hydrogel-type hemostats. Moreover, profited from the excellent biocompatibility and bioactivity of ECM, the material enhances angiogenesis and endothelial cell functions. *In vivo* experiments reveal that the ECM-based powders have excellent hemostasis effects in multifarious rabbit non-compressible and massive hemorrhage models, which can quickly self-assemble to seal the bleeding site and greatly halt blood loss. More importantly, as the material biodegrades *in vivo*, the inherent biological cues can induce the vessels and bile ducts formation in defected liver, promoting in situ tissue functional repair after hemostasis.

In summary, the comprehensive results support the high application potential of all-in-one ECM-based powders in many fields. Due to the significant advantages of portability and ease of use, it is of great application value and provides a competitive solution in dealing with emergencies such as battlefield, natural disaster, traffic accident and so on. Given the versatile bioactivities and tissue repair ability, the ECM-based hemostatic powder has shown a broad application prospect in many clinical fields such as skin wound repair, closure and repair of damaged organs, and even in endoscopic-related surgeries.

4. Materials and methods

4.1. Preparation of the modified SIS and SA

The SIS (i.e., decellularized porcine small intestine submucosa) was prepared according to the previously described procedures [30]. Briefly, market-sourced fresh porcine small intestines underwent mechanical excision of the tunica serosa and tunica muscularis. And following a multi-step decellularization process and lyophilization, the SIS membranes were obtained. Hydroxylated SIS (SIS-OH) is prepared using enzymatic-digested SIS solution by convenient amidation reaction. Finally, the resultant product is obtained by dialysis and lyophilization. The details are provided in the Supporting Information.

A two-step process was designed to synthesize ADA-PBA. Firstly, aldehydeated sodium alginate (ADA) was prepared by oxidation reaction based on the strong oxidation property of $NaIO_4$. Secondly, ADA and 3-aminophenylboronic acid (PBA) were reacted under the catalysis of EDC. Finally, the ADA-PBA was gained after dialysis and lyophilization outlined earlier. The details are provided in the Supporting Information.

4.2. Preparation of the ECM-based powders

The ECM-based powder was conveniently prepared by freeze-drying and physical grinding of hydrogel. Initially, SIS-OH and ADA-PBA were individually dissolved in PBS, with concentrations of 5 % and 10 %, respectively. Subsequently, these two solutions were combined in a 1 : 2 vol ratio, ensuring a uniform mixture. To form ECM-based hydrogels, the pH of the mixture was carefully adjusted to 7–8 using an alkali solution. The freeze-dried ECM-based hydrogel was ground by grinder (70 Hz, 45 s, 3 times) to prepare powder. In this study, three kinds of ECM-based materials (AP, APS and APSO powders) with different components were prepared.

4.3. Chemical structure and morphology of materials

The chemical structure of SIS-OH and ADA-PBA were determined by FTIR (INVENIO R, Bruker). That of APSO hydrogel after self-assembly was determined by FTIR (INVENIO R, Bruker) and XPS (C 1s 284.6 eV, Axis Ultra DLD, Kratos). The materials morphology and elements distribution were observed using SEM (SU3500, Hitachi) and EDS (Aztec X-Max20, Oxford) respectively. Additionally, the representative powder-type hemostatic products were also used for comparison, including Celox™, Zeolite and Yunnan Baiyao powder (YB). And the average size of hemostatic powders was analyzed according to the SEM images using Image J software (n = 30). All samples are required gold spraying to enhance electrical conductivity. The details are provided in the Supporting Information.

4.4. Liquid absorption and rapid self-assembly capacity

PBS and anticoagulant blood (3.8 wt% sodium citrate solution: blood = 1 : 9, v/v) were used as the representative liquid to evaluate the liquid absorption capacity of the Celox™, Zeolite, YB, AP, APS and APSO powders. The liquid absorption (wt%) of the powders were quantified, and the speed of water absorption was evaluated by the 30s/5s liquid absorption (%) (n = 3). Moreover, the liquid absorption process of hemostatic powders was recorded by optical static contact angle measuring instrument (DSA25, KRUSS). The rapid self-assembly ability of the powder was evaluated with an inverted tube method. The APSO powder was introduced into a tube with anticoagulant blood and turned over it after 5 s, then the tube was observed and photographed. The Celox™, YB and Zeolite powders were used as the comparation. The details are provided in the Supporting Information.

4.5. Rheology and bio-adhesion properties evaluation

All the rheology tests were performed via a rotational rheometer (Physica MCR302, Anton Paar) with plate rotor (PP25-3) with a 0.5 mm gap size. The frequency sweep mode (0.1–100 Hz), the strain sweep mode (1–300 %) and the alternate step strain sweep with the cyclic strain (low strain: 1 %, high strain: 300 %) were carried out to characterize the rheological properties of the samples. The details are provided in the Supporting Information.

The wet bio-adhesion property of AP, APS and APSO powders was initially assessed via tensile test carried out by an universal mechanical test machine (Instron 5967, USA) (n = 3). Meanwhile, the commercial fibrin glue (Guangzhou Bioseal Biotech Co., Ltd., China) was selected for testing following the manufacturer's instructions. The assessment of the bio-adhesive capability in wet conditions was conducted through wet pigskin adhesion experiment and heavy lifting test. The whole processes were recorded using electronic devices. Then, the interface between hydrogel and pigskin was observed by SEM. The details are provided in the Supporting Information.

4.6. Biocompatibility of the ECM-based powders

Human umbilical vein endothelial cells (HUVECs), NIH-3T3 and bone marrow-derived stem cells (BMSCs) were used to evaluate the material's cytocompatibility. The effect of materials on cell viability and proliferation was assessed using a live/dead staining kit (40747ES76, Yeasen, China) and CCK-8 assay (40203ES80, Yeasen, China), respectively. The complete medium was used as a control. The hemocompatibility of the material was determined using a hemolysis test, and the saline and 0.1 % Triton X-100 had served as negative and positive controls, respectively (n = 3). The histocompatibility was estimated by subcutaneous implantation in rats. The details are provided in the Supporting Information.

4.7. Enhanced cell recruitment evaluation

The scratch assay and Transwell migration method were used to assess the effect of material extract on the cell recruitment. For the former, the HUVECs were seeded onto 6-well culture plates. After

reaching the desired confluency, a straight scratch was created after serum starvation. Subsequently, the original medium was replaced with material conditioned medium, with images captured over time. Complete culture medium without serum was used as a control. The optical microscope images were captured at 24 and 48 h, and the migration rate was calculated (n = 3). For Transwell migration method, The HUVECs, NIH-3T3 and BMSCs were then seeded into the upper chamber, while conditioned medium containing different ECM-based materials was added to the lower chamber. After 24 h, the cells in lower chamber were fixed, stained with 0.5 % crystal violet (Beyotime, China), and photographed. The migrated cells were quantified using Image J software (n = 3). The details are provided in the Supporting Information.

4.8. Angiogenesis and enhanced HUVECs functions evaluation

Tube formation assay was carried out to evaluate the angiogenesis of AP, APS and APSO. The HUVECs were seeded on gelated Matrigel (Sigma, USA), which cultured under different material conditioned medium. After incubation for 3, 6 and 9 h, the situation of tube formation was photographed. To further assess tube formation capability, the total length and number of mesh were analyzed using Image J software (n = 3). The NO and prostaglandin-I-2 (PGI_2) level were assessed using NO fluorescence probe (DAF-FM DA, 40769ES50, Yeasen, China) and enzyme linked immunosorbent assay (ELISA), respectively. The details are provided in the Supporting Information.

Genes critical to the function of angiogenesis and endothelial cells are detected by RT-qPCR. The relative level of *Egf*, *Vegf-a*, *bFgf*, *eNos*, *Ang-2* and *Hif-1α* expression was expressed as $2^{-\Delta\Delta Ct}$, and *Gapdh* served as a housekeeping gene for the normalization of data (n = 3). The primers sequences are listed in Table S1. The details are provided in the Supporting Information.

4.9. Hemostasis performance in vivo

The animal experiments in this study were approved by the Animal Protection and Use Committee of Sichuan University (No. 20240718005 and 20230120001), and the relevant ethical guidelines were strictly observed during the experiment.

The hemostatic ability of ECM-based powder was evaluated by using the model of non-compressible hemorrhage in rabbit liver volume defect. Male New Zealand white rabbits weighing 2.5–3.0 kg were anesthetized with pentobarbital sodium (1.1 mL kg^{-1}). A deep defect with a diameter of 10 mm and a depth of 5 mm was constructed on the lobus dexter lateralis of rabbit liver with a biopsy to build a of liver injury hemorrhage model. Hemostasis was immediately performed with Celox™, AP, APS and APSO powders, and the blank group was not treated with hemostasis. The hemostasis process was recorded, and the outgoing blood is collected with a clean filter paper to estimate blood loss. For building the rabbit cardiac perforation model massive hemorrhage, the rabbit right ventriculus dexter was perforated with a 50 mL syringe needle after the heart expose, and APSO and Celox™ powders were applied. In addition, the blood flow in separated femoral artery was blocked with two clamps, perforated by 2 mL syringe. The APSO powder was used and in situ self-assembly using PBS, and the control group was covered with gauze, the blood loss was recorded within 5 min of restoring blood flow.

In order to further explore the process of hemostasis, the bleeding sites of rabbits were collected after euthanasia following being observed by SEM after fixation with paraformaldehyde, gradient dehydration, critical point drying, and gold spraying. Furthermore, the fixed liver samples were paraffin embedded, sectioned, dewaxed and rehydrated for H&E staining.

4.10. In-situ liver defect repair

The liver repair after hemostasis ability of ECM-based powder was evaluated by using the model of non-compressible bleeding in rabbit liver volume defect consistent with the above. After hemostasis, the abdomen was sutured, and the rabbits were feed to order. ESU group performed hemostasis with electric knife, and other operations were the same as before. The electric knife was selected as the coagulation mode, the power of the electric knife was adjusted, and the electric knife was used to stop bleeding in the defect of the liver, and meanwhile minimizes damage to surrounding tissues.

4.11. Histological and hematological analysis

Rabbits were euthanized on postoperative day 14 and 28, and liver was fixed in 10 % neutral buffered formalin. The embedded liver samples were sliced for subsequent histological evaluation. H&E staining was used to assess tissue repair. Sirius red staining was used to visualize the deposition of collagen fibers. Liver glycogen expression in the regenerating area was assessed by PAS staining. Furthermore, IHC staining of CD31 (11265-1-AP, 1 : 2000, Proteintech) and CK19 (ab220193, 1 : 150, Abcam) was used to assess neovascularization and nascent bile ducts, respectively. The details are provided in the Supporting Information.

On postoperative day 14 and 28, the blood in the ear artery was collected after disinfection using the blood collection needles. Blood was injected into the blood vessel collection for blood routine and blood biochemical test according to the manufacturer's instructions. The processed blood samples were sent to West China-Frontier Pharma Tech for testing.

4.12. Statistical analysis

All data were presented in the form of mean ± standard deviation. Statistical analysis was carried out utilizing software (GraphPad Prism, v8.0). The statistical significance between two groups was evaluated through Student's t-test, while one-way ANOVA was employed to assess significance among multiple groups. *P* value less than 0.05 was deemed statistically significant. ($^*P < 0.05$, $^{**}P < 0.01$, $^{***}P < 0.001$, $^{****}P < 0.0001$).

CRediT authorship contribution statement

Chen-Yu Zou: Writing – original draft, Visualization, Methodology, Conceptualization. **Chen Han:** Writing – original draft, Visualization, Methodology. **Ming Xiong:** Visualization, Methodology. **Juan-Juan Hu:** Visualization, Methodology. **Yan-Lin Jiang:** Visualization, Methodology. **Xiu-Zhen Zhang:** Visualization, Methodology. **Ya-Xing Li:** Visualization, Validation, Investigation. **Long-Mei Zhao:** Validation, Formal analysis. **Yu-Ting Song:** Visualization, Methodology. **Qing-Yi Zhang:** Visualization, Validation, Methodology. **Qian-Jin Li:** Visualization, Investigation. **Rong Nie:** Validation, Investigation. **Yue-Qi Zhang:** Visualization, Investigation. **Jesse Li-Ling:** Validation, Investigation. **Hui-Qi Xie:** Writing – review & editing, Writing – original draft, Supervision, Conceptualization.

Ethics approval and consent to participate

The animal experiments in this study were approved by the Animal Protection and Use Committee of Sichuan University (No. 20240718005 and 20230120001), and the relevant ethical guidelines were strictly observed during the experiment.

Declaration of competing interest

The authors declare that they have no known competing financial interests or personal relationship which could have appeared to influence the work reported in this paper.

Acknowledgement

Chen-Yu Zou and Chen Han have contributed equally to this work. This study has been jointly sponsored by Sichuan Science and Technology Program (2024NSFSC0002 and MZGC20240011), the National Natural Science Foundation of China (324B2047), "1.3.5" Project for Disciplines of Excellence, West China Hospital, Sichuan University (ZYGD23037), and the Frontiers Medical Center, Tianfu Jincheng Laboratory Foundation (TFJC2023010002). The authors thank Dai-Bing Luo (Analytical & Testing Center, Sichuan University), Mao-Jia Chen and Jie-Hao Chen (Animal Laboratory Center, West China Hospital, Sichuan University) for the support in mechanical testing and animal experiment, respectively.

Appendix A. Supplementary data

Supplementary data to this article can be found online at https://doi.org/10.1016/j.bioactmat.2025.04.005.

References

[1] H. He, W. Zhou, J. Gao, F. Wang, S. Wang, Y. Fang, Y. Gao, W. Chen, W. Zhang, Y. Weng, Z. Wang, H. Liu, Efficient, biosafe and tissue adhesive hemostatic cotton gauze with controlled balance of hydrophilicity and hydrophobicity, Nat. Commun. 13 (1) (2022) 552, https://doi.org/10.1038/s41467-022-28209-8.

[2] Y. Yang, G. He, Z. Pan, K. Zhang, Y. Xian, Z. Zhu, Y. Hong, C. Zhang, D. Wu, An injectable hydrogel with ultrahigh burst pressure and innate antibacterial activity for emergency hemostasis and wound repair, Adv. Mater. 36 (33) (2024) e2404811, https://doi.org/10.1002/adma.202404811.

[3] T. Jiang, S. Chen, J. Xu, Y. Zhang, H. Fu, Q. Ling, Y. Xu, X. Chu, R. Wang, L. Hu, H. Li, W. Huang, L. Bian, P. Zhao, F. Wei, Superporous sponge prepared by secondary network compaction with enhanced permeability and mechanical properties for non-compressible hemostasis in pigs, Nat. Commun. 15 (1) (2024) 5460, https://doi.org/10.1038/s41467-024-49578-2.

[4] X. Zhao, Y. Huang, Z. Li, J. Chen, J. Luo, L. Bai, H. Huang, E. Cao, Z. Yin, Y. Han, B. Guo, Injectable self-expanding/self-propelling hydrogel adhesive with procoagulant activity and rapid gelation for lethal massive hemorrhage management, Adv. Mater. 36 (15) (2024) e2308701, https://doi.org/10.1002/adma.202308701.

[5] K. Yao, S. Li, X. Zheng, Q. Zhang, J. Liu, C. Liang, K. Duan, J. Ye, Y. Yin, X. Chen, Superwettable calcium ion exchanged carboxymethyl cellulose powder with self-gelation, tissue adhesion and bioabsorption for effective hemorrhage control, Chem. Eng. J. 481 (2024) 148770, https://doi.org/10.1016/j.cej.2024.148770.

[6] X.X. Lei, C.Y. Zou, J.J. Hu, M.H. Fan, Y.L. Jiang, M. Xiong, C. Han, X.Z. Zhang, Y. X. Li, L.M. Zhao, R. Nie, J. Li-Ling, H.Q. Xie, A self-assembly pro-coagulant powder capable of rapid gelling transformation and wet adhesion for the efficient control of non-compressible hemorrhage, Adv. Sci. 11 (4) (2023) e2306289, https://doi.org/10.1002/advs.202306289.

[7] F. Leng, F. Chen, X. Jiang, Modified porous carboxymethyl chitin microspheres by an organic solvent-free process for rapid hemostasis, Carbohydr. Polym. 270 (2021) 118348, https://doi.org/10.1016/j.carbpol.2021.118348.

[8] P. Shi, X. He, H. Cong, B. Yu, Y. Shen, Preparation and properties of self-assembling polypeptide hydrogels and their application in biomedicine, ACS Mater. Lett. 6 (5) (2024) 1649–1677, https://doi.org/10.1021/acsmaterialslett.3c01546.

[9] J. Kim, S. Lee, Y. Kim, M. Choi, I. Lee, E. Kim, C.G. Yoon, K. Pu, H. Kang, J.S. Kim, In situ self-assembly for cancer therapy and imaging, Nat. Rev. Mater. 8 (11) (2023) 710–725, https://doi.org/10.1038/s41578-023-00589-3.

[10] C. Hui, Y. Gao, B.-Y. Yan, L.-Q. Ding, T.-C. Sun, Z. Liu, S. Ramakrishna, Y.-Z. Long, J. Zhang, Collocalia birds inspired Janus-structured bandage with strong wet tissue adhesion for rapid hemostasis and wound healing, Chem. Eng. J. 464 (2023) 142458, https://doi.org/10.1016/j.cej.2023.142458.

[11] M. Lee, D. Seo, J. Park, S.H. Lee, J. Jeon, W. Kim, J. Kim, H.S. Yang, J.Y. Lee, Wet tissue adhesive polymeric powder hydrogels for skeletal muscle regeneration, Bioact. Mater. 40 (2024) 334–344, https://doi.org/10.1016/j.bioactmat.2024.06.017.

[12] Y. Fang, L. Zhang, Y. Chen, S. Wu, Y. Weng, H. Liu, Polysaccharides based rapid self-crosslinking and wet tissue adhesive hemostatic powders for effective hemostasis, Carbohydr. Polym. 312 (2023) 120819, https://doi.org/10.1016/j.carbpol.2023.120819.

[13] B. Li, H. Li, H. Chen, Y. Liu, J. Chen, Q. Feng, X. Cao, H. Dong, Microgel assembly powder improves acute hemostasis, antibacterial, and wound healing via in situ Co-assembly of erythrocyte and microgel, Adv. Funct. Mater. 33 (36) (2023) 2302793, https://doi.org/10.1002/adfm.202302793.

[14] X. Peng, X. Xu, Y. Deng, X. Xie, L. Xu, X. Xu, W. Yuan, B. Yang, X. Yang, X. Xia, L. Duan, L. Bian, Ultrafast self-gelling and wet adhesive powder for acute hemostasis and wound healing, Adv. Funct. Mater. 31 (33) (2021) 2102583, https://doi.org/10.1002/adfm.202102583.

[15] K. Zhang, Y. Xian, M. Li, Z. Pan, Z. Zhu, Y. Yang, H. Wang, L. Zhang, C. Zhang, D. Wu, Gelable and adhesive powder for lethal non-compressible hemorrhage control, Adv. Funct. Mater. 33 (46) (2023) 2305222, https://doi.org/10.1002/adfm.202305222.

[16] Y. Liang, M. Li, Y. Yang, L. Qiao, H. Xu, B. Guo, pH/glucose dual responsive metformin release hydrogel dressings with adhesion and self-healing via dual-dynamic bonding for athletic diabetic foot wound healing, ACS Nano 16 (2) (2022) 3194–3207, https://doi.org/10.1021/acsnano.1c11040.

[17] R. Li, K. Liu, X. Huang, D. Li, J. Ding, B. Liu, X. Chen, Bioactive materials promote wound healing through modulation of cell behaviors, Adv. Sci. 9 (10) (2022) e2105152, https://doi.org/10.1002/advs.202105152.

[18] X.-X. Lei, C.-Y. Zou, J.-J. Hu, Y.-L. Jiang, X.-Z. Zhang, L.-M. Zhao, T. He, Q.-Y. Zhang, Y.-X. Li, J. Li-Ling, H.-Q. Xie, Click-crosslinked in-situ hydrogel improves the therapeutic effect in wound infections through antibacterial, antioxidant and anti-inflammatory activities, Chem. Eng. J. 461 (2023) 142092, https://doi.org/10.1016/j.cej.2023.142092.

[19] C.Y. Zou, Q.J. Li, J.J. Hu, Y.T. Song, Q.Y. Zhang, R. Nie, J. Li-Ling, H.Q. Xie, Design of biopolymer-based hemostatic material: starting from molecular structures and forms, Materials Today Bio 17 (2022) 100468, https://doi.org/10.1016/j.mtbio.2022.100468.

[20] B. Guo, R. Dong, Y. Liang, M. Li, Haemostatic materials for wound healing applications, Nat. Rev. Chem 5 (11) (2021) 773–791, https://doi.org/10.1038/s41570-021-00323-z.

[21] X. Zhang, X. Chen, H. Hong, R. Hu, J. Liu, C. Liu, Decellularized extracellular matrix scaffolds: recent trends and emerging strategies in tissue engineering, Bioact. Mater. 10 (2022) 15–31, https://doi.org/10.1016/j.bioactmat.2021.09.014.

[22] L.T. Saldin, M.C. Cramer, S.S. Velankar, L.J. White, S.F. Badylak, Extracellular matrix hydrogels from decellularized tissues: structure and function, Acta Biomater. 49 (2017) 1–15, https://doi.org/10.1016/j.actbio.2016.11.068.

[23] W. Wang, X. Zhang, N.N. Chao, T.W. Qin, W. Ding, Y. Zhang, J.W. Sang, J.C. Luo, Preparation and characterization of pro-angiogenic gel derived from small intestinal submucosa, Acta Biomater. 29 (2016) 135–148, https://doi.org/10.1016/j.actbio.2015.10.013.

[24] Y.L. Jiang, Z.L. Wang, Z.X. Fan, M.J. Wu, Y. Zhang, W. Ding, Y.Z. Huang, H.Q. Xie, Human adipose-derived stem cell-loaded small intestinal submucosa as a bioactive wound dressing for the treatment of diabetic wounds in rats, Biomater. Adv. 136 (2022) 212793, https://doi.org/10.1016/j.bioadv.2022.212793.

[25] Q.-Y. Zhang, J. Tan, R. Nie, Y.-T. Song, X.-L. Zhou, Z.-Y. Feng, K. Huang, C.-Y. Zou, Q.-J. Yuan, L.-M. Zhao, X.-Z. Zhang, Y.-L. Jiang, L.-M. Liu, J. Li-Ling, H.-Q. Xie, Acceleration of wound healing by composite small intestinal submucosa hydrogels through immunomodulation, Compos. B Eng. 254 (2023) 110550, https://doi.org/10.1016/j.compositesb.2023.110550.

[26] L.P. Huang, Y. Liu, Q.J. Li, W.Q. Zhang, C.Y. Wu, L.M. Zhao, H.Q. Xie, A modified small intestinal submucosa patch with multifunction to promote scarless repair and reinvigoration of urethra, Adv. Healthcare Mater. 12 (23) (2023) 2300519, https://doi.org/10.1002/adhm.202300519.

[27] N. Sheng, F. Xing, Q.-Y. Zhang, J. Tan, R. Nie, K. Huang, H.-X. Li, Y.-L. Jiang, B. Tan, Z. Xiang, H.-Q. Xie, A pleiotropic SIS-based hydrogel with immunomodulation via NLRP3 inflammasome inhibition for diabetic bone regeneration, Chem. Eng. J. 480 (2024) 147985, https://doi.org/10.1016/j.cej.2023.147985.

[28] J.-J. Hu, X.-X. Lei, Y.-L. Jiang, C.-Y. Zou, Y.-T. Song, C.-Y. Wu, L.-Q. Tang, D. Lu, J. Li-Ling, H. Yang, H.-Q. Xie, Scarless vocal fold regeneration by urine-derived stem cells and small intestinal submucosa hydrogel composites through enhancement of M2 macrophage Polarization, neovascularization and Re-epithelialization, Smart Materials in Medicine 3 (2022) 339–351, https://doi.org/10.1016/j.smaim.2022.04.002.

[29] J. Tan, Q.-Y. Zhang, Y.-T. Song, K. Huang, Y.-L. Jiang, J. Chen, R. Wang, C.-Y. Zou, Q.-J. Li, B.-Q. Qin, N. Sheng, R. Nie, Z.-Y. Feng, D.-Z. Yang, W.-H. Yi, H.-Q. Xie, Accelerated bone defect regeneration through sequential activation of the M1 and M2 phenotypes of macrophages by a composite BMP-2@SIS hydrogel: an immunomodulatory perspective, Compos. B Eng. 243 (2022) 110149, https://doi.org/10.1016/j.compositesb.2022.110149.

[30] Y.-T. Song, L. Dong, J.-G. Hu, P.-C. Liu, Y.-L. Jiang, L. Zhou, M. Wang, J. Tan, Y.-X. Li, Q.-Y. Zhang, C.-Y. Zou, X.-Z. Zhang, L.-M. Zhao, R. Nie, Y. Zhang, J. Li-Ling, H.-Q. Xie, Application of genipin-crosslinked small intestine submucosa and urine-derived stem cells for the prevention of intrauterine adhesion in a rat model, Compos. B Eng. 250 (2023) 110461, https://doi.org/10.1016/j.compositesb.2022.110461.

[31] L.-M. Zhao, L.-C. Da, R. Wang, L. Wang, Y.-L. Jiang, X.-Z. Zhang, Y.-X. Li, X.-X. Lei, Y.-T. Song, C.-Y. Zou, L.-P. Huang, W.-Q. Zhang, Q.-Y. Zhang, Q.-J. Li, R. Nie, Y. Zhang, Y. Liang, J. Li-Ling, H.-Q. Xie, Promotion of uterine reconstruction by a tissue-engineered uterus with biomimetic structure and extracellular matrix microenvironment, Sci. Adv. 9 (46) (2023), https://doi.org/10.1126/sciadv.adi6488 eadi6488.

[32] X.Z. Zhang, Y.L. Jiang, J.G. Hu, L.M. Zhao, Q.Z. Chen, Y. Liang, Y. Zhang, X.X. Lei, R. Wang, Y. Lei, Q.Y. Zhang, J. Li-Ling, H.Q. Xie, Procyanidins-crosslinked small intestine submucosa: a bladder patch promotes smooth muscle regeneration and bladder function restoration in a rabbit model, Bioact. Mater. 6 (6) (2021) 1827–1838, https://doi.org/10.1016/j.bioactmat.2020.11.023.

[33] R. Nie, Q.-Y. Zhang, J. Tan, Z.-Y. Feng, K. Huang, N. Sheng, Y.-L. Jiang, Y.-T. Song, C.-Y. Zou, L.-M. Zhao, H.-X. Li, R. Wang, X.-L. Zhou, J.-J. Hu, C.-Y. Wu, J. Li-Ling, H.-Q. Xie, EGCG modified small intestine submucosa promotes wound healing through immunomodulation, Compos. B Eng. 267 (2023) 111005, https://doi.org/10.1016/j.compositesb.2023.111005.

[34] J. Zhang, B. Gao, B. Ye, Z. Sun, Z. Qian, L. Yu, Y. Bi, L. Ma, Y. Ding, Y. Du, W. Wang, Z. Mao, Mitochondrial-targeted delivery of polyphenol-mediated

antioxidases complexes against pyroptosis and inflammatory diseases, Advanced Material 35 (11) (2023) e2208571, https://doi.org/10.1002/adma.202208571.
[35] K. Kim, J.H. Ryu, M.-Y. Koh, S.P. Yun, S. Kim, J.P. Park, C.-W. Jung, M.S. Lee, H.-I. Seo, J.H. Kim, H. Lee, Coagulopathy-independent, bioinspired hemostatic materials: a full research story from preclinical models to a human clinical trial, Sci. Adv. 7 (13) (2021) eabc9992, https://doi.org/10.1126/sciadv.abc9992.
[36] S. Bian, L. Hao, X. Qiu, J. Wu, H. Chang, G.M. Kuang, S. Zhang, X. Hu, Y. Dai, Z. Zhou, F. Huang, C. Liu, X. Zou, W. Liu, W.W. Lu, H. Pan, X. Zhao, An injectable rapid-adhesion and anti-swelling adhesive hydrogel for hemostasis and wound sealing, Adv. Funct. Mater. 32 (46) (2022) 2207741, https://doi.org/10.1002/adfm.202207741.
[37] V.G. Muir, J.A. Burdick, Chemically modified biopolymers for the formation of biomedical hydrogels, Chem. Rev. 121 (18) (2021) 10908–10949, https://doi.org/10.1021/acs.chemrev.0c00923.
[38] E. Zhang, J. Yang, K. Wang, B. Song, H. Zhu, X. Han, Y. Shi, C. Yang, Z. Zeng, Z. Cao, Biodegradable zwitterionic cream gel for effective prevention of postoperative adhesion, Adv. Funct. Mater. 31 (10) (2020) 2009431, https://doi.org/10.1002/adfm.202009431.
[39] J. Park, T.Y. Kim, Y. Kim, S. An, K.S. Kim, M. Kang, S.A. Kim, J. Kim, J. Lee, S. W. Cho, J. Seo, A mechanically resilient and tissue-conformable hydrogel with hemostatic and antibacterial capabilities for wound care, Adv. Sci. 10 (30) (2023) e2303651, https://doi.org/10.1002/advs.202303651.
[40] M. Beudert, M. Gutmann, T. Luhmann, L. Meinel, Fibrin sealants: challenges and solutions, ACS Biomater. Sci. Eng. 8 (6) (2022) 2220–2231, https://doi.org/10.1021/acsbiomaterials.1c01437.
[41] R. Song, X. Wang, M. Johnson, C. Milne, A. Lesniak-Podsiadlo, Y. Li, J. Lyu, Z. Li, C. Zhao, L. Yang, I. Lara-Sáez, S. A, W. Wang, Enhanced strength for double network hydrogel adhesive through cohesion-adhesion balance, Adv. Funct. Mater. 34 (23) (2024) 2313322, https://doi.org/10.1002/adfm.202313322.
[42] C.Y. Zou, X.X. Lei, J.J. Hu, Y.L. Jiang, Q.J. Li, Y.T. Song, Q.Y. Zhang, J. Li-Ling, H. Q. Xie, Multi-crosslinking hydrogels with robust bio-adhesion and pro-coagulant activity for first-aid hemostasis and infected wound healing, Bioact. Mater. 16 (2022) 388–402, https://doi.org/10.1016/j.bioactmat.2022.02.034.
[43] C.-Y. Zou, J.-J. Hu, D. Lu, Q.-J. Li, Y.-L. Jiang, R. Wang, H.-Y. Wang, X.-X. Lei, J. Li-Ling, H. Yang, H.-Q. Xie, A self-fused hydrogel for the treatment of glottic insufficiency through outstanding durability, extracellular matrix-inducing bioactivity and function preservation, Bioact. Mater. 24 (2023) 54–68, https://doi.org/10.1016/j.bioactmat.2022.12.006.
[44] Y. Wu, Y. Wang, C. Zheng, C. Hu, L. Yang, Q. Kong, H. Zhang, Y. Wang, A versatile glycopeptide hydrogel promotes chronic refractory wound healing through bacterial elimination, sustained oxygenation, immunoregulation, and neovascularization, Adv. Funct. Mater. 33 (49) (2023) 2305992, https://doi.org/10.1002/adfm.202305992.
[45] H. Wu, L. Yang, R. Luo, L. Li, T. Zheng, K. Huang, Y. Qin, X. Yang, X. Zhang, Y. Wang, A drug-free cardiovascular stent functionalized with tailored collagen supports in-situ healing of vascular tissues, Nat. Commun. 15 (1) (2024) 735, https://doi.org/10.1038/s41467-024-44902-2.
[46] B. Wang, H. Shen, Y. Wei, F. Liu, Y. Yang, H. Yu, J. Fu, X. Cui, T. Yu, Y. Xu, Y. Liu, H. Dong, F. Shen, W. Zhou, H. Liu, Y. Chen, H. Wang, Balance of Gata3 and Ramp2 in hepatocytes regulates hepatic vascular reconstitution in postoperative liver regeneration, J. Hepatol. 80 (2) (2024) 309–321, https://doi.org/10.1016/j.jhep.2023.10.016.
[47] Y. Li, J. Zhu, X. Zhang, Y. Li, S. Zhang, L. Yang, R. Li, Q. Wan, X. Pei, J. Chen, J. Wang, Drug-delivery nanoplatform with synergistic regulation of angiogenesis–osteogenesis coupling for promoting vascularized bone regeneration, ACS Appl. Mater. Interfaces 15 (14) (2023) 17543–17561, https://doi.org/10.1021/acsami.2c23107.
[48] Y. Guo, Y. Wang, X. Zhao, X. Li, Q. Wang, W. Zhong, K. Mequanint, R. Zhan, M. Xing, G. Luo, Snake extract–laden hemostatic bioadhesive gel cross-linked by visible light, Sci. Adv. 7 (29) (2021) eabf9635, https://doi.org/10.1126/sciadv.abf9635.
[49] R. Dong, H. Zhang, B. Guo, Emerging hemostatic materials for non-compressible hemorrhage control, Natl. Sci. Rev. 9 (11) (2022) nwac162, https://doi.org/10.1093/nsr/nwac162.
[50] C.-Y. Zou, C. Han, F. Xing, Y.-L. Jiang, M. Xiong, J. Li-Ling, H.-Q. Xie, Smart design in biopolymer-based hemostatic sponges: from hemostasis to multiple functions, Bioact. Mater. 45 (2025) 459–478, https://doi.org/10.1016/j.bioactmat.2024.11.034.
[51] L. Qi, L. Mu, X. Guo, A. Liu, C. Chen, Q. Ye, Z. Zhong, X. Shi, Fast expandable chitosan-fibers cryogel from ambient drying for noncompressible bleeding control and in situ tissue regeneration, Adv. Funct. Mater. 33 (16) (2023) 2212231, https://doi.org/10.1002/adfm.202212231.
[52] H. Wei, F. Li, T. Xue, H. Wang, E. Ju, M. Li, Y. Tao, MicroRNA-122-functionalized DNA tetrahedron stimulate hepatic differentiation of human mesenchymal stem cells for acute liver failure therapy, Bioact. Mater. 28 (2023) 50–60, https://doi.org/10.1016/j.bioactmat.2023.04.024.
[53] M. Kharaziha, T. Scheibel, S. Salehi, Multifunctional naturally derived bioadhesives: from strategic molecular design toward advanced biomedical applications, Prog. Polym. Sci. 150 (2024) 101792, https://doi.org/10.1016/j.progpolymsci.2024.101792.
[54] C. Drakeford, S. Aguila, F. Roche, K. Hokamp, J. Fazavana, M.P. Cervantes, A. M. Curtis, H.C. Hawerkamp, S.P.S. Dhami, H. Charles-Messance, E.E. Hackett, A. Chion, S. Ward, A. Ahmad, I. Schoen, E. Breen, J. Keane, R. Murphy, R.J. S. Preston, J.M. O'Sullivan, F.J. Sheedy, P. Fallon, J.S. O'Donnell, von Willebrand factor links primary hemostasis to innate immunity, Nat. Commun. 13 (1) (2022) 6320, https://doi.org/10.1038/s41467-022-33796-7.
[55] H. Liu, Z. Cai, F. Wang, H. Ruan, C. Zhang, J. Zhong, Z. Wang, W. Cui, Platelet membrane fragment self-assembled oral hydrogel microspheres for restoring intestinal microvascular injury, Adv. Funct. Mater. 33 (33) (2023) 2302007, https://doi.org/10.1002/adfm.202302007.
[56] L. Xiao, Y. Ma, R. Crawford, J. Mendhi, Y. Zhang, H. Lu, Q. Zhao, J. Cao, C. Wu, X. Wang, Y. Xiao, The interplay between hemostasis and immune response in biomaterial development for osteogenesis, Mater. Today 54 (2022) 202–224, https://doi.org/10.1016/j.mattod.2022.02.010.